Master's thesis

NTNU
Norwegian University of Science and Technology
Faculty of Engineering
Department of Energy and Process Engineering

Henrik Andreas Mortensen

Digital Compressor System

Master's thesis in Mechanical Engineering
Supervisor: Professor, Lars Eirik Bakken
June 2020

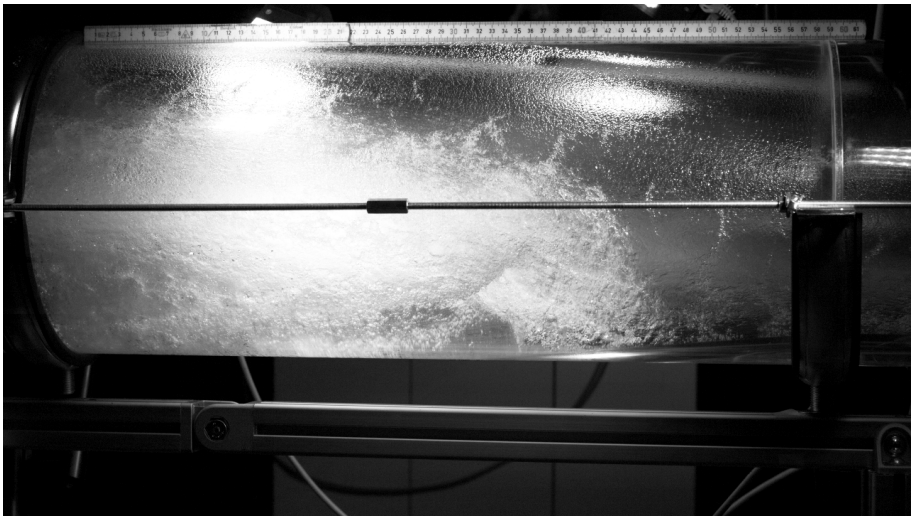

NTNU
Norwegian University of
Science and Technology

Henrik Andreas Mortensen

Digital Compressor System

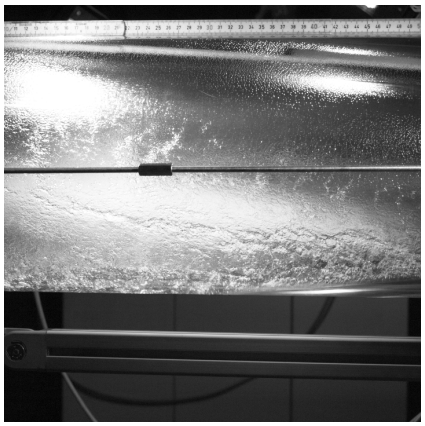

Master's thesis in Mechanical Engineering
Supervisor: Professor, Lars Eirik Bakken
June 2020

Norwegian University of Science and Technology
Faculty of Engineering
Department of Energy and Process Engineering

NTNU
Norwegian University of
Science and Technology

Norwegian University of Science and Technology

Faculty of Engineering
Department of Energy and Process Engineering

EPT-P-2020

NTNU

MASTER WORK

for

student Henrik Andreas Mortensen

Spring 2020

Digital Compressor System

Background and objective

Condition monitoring is an important aspect to ensure safe and efficient operation of turbomachinery. Especially this relates to low and/or unmanned operation where access to relevant operational parameters may be limited.

The overall objective is to test and analyse new technologies and explore opportunities within compressor digitalization methods. Based on the NTNU test lab compressor, including the new inlet venturi-tube element, a digital twin model should be established to explore the interaction between the venturi-tube and the compressor.

The following tasks to be considered:

Based on literature review and experimental work at the wet gas compressor test rig, the focus areas are:

1. Establish relevant compressor performance characteristics.

2. Review and validate the venturi-tube behaviour at wet gas conditions.

3. Establish and document a digital model of the interaction between the compressor and venturi-tube at different operating conditions. Focus may be given to sudden shift in venturi-tube behaviour.

Supervisor:

Lars E Bakken

Co-Supervisor(s):

Olav Mehlum, Equinor
Erik Langørgen, NTNU
Øyvind Hundseid, NTNU

Address
N-7034 Trondheim
Norway

Location
K. Hejes vei 1b

Tel. +47 73 59 38 60
Fax +47 73 59 35 80
Org. no. NO 974 767 880

Preface

This master thesis, titled "Digital Compressor Modelling" is a part of a Master of Science program in Mechanical Engineering at the Norwegian University of Science and Technology (NTNU). It was written during the spring semester of 2020 comprising a workload of 30 ECTS credits.

I want to thank my supervisor Professor Lars Eirik Bakken for his advice and teaching during the thesis and my Co-Supervisor Erik Langørgen for guidance with the compressor system and for ruining the compressor laboratory. Special thanks to my fellow students at the study hall B126 for the companionship and discussions over coffee breaks. I want to thank the Norwegian people for their admirable "dugnads ånd" during a trying time while the Covid-19 pandemic plague the world.

Lastly, I want to end with some words that have help me through this trying time of isolation.

> *"Loneliness does not come from having no people about one, but from being unable to communicate the things that seem important to oneself, or from holding certain views which others find inadmissible."*
>
> Carl Gustav Jung

Trondheim, 24-06-2020

Henrik Andreas Mortensen

Abstract

Subsea wet gas compression has been used to increase the recovery rate of gas fields for a few years now. It has a large potential to further increase production and cut costs. Although, wet gas compression is still in its infancy and requires further development to make the systems more reliable, economic and commercially viable.

Venturis have been utilized to determine flow in a system since 1895 and is now one of the most common methods for flow measurements. While the venturi effect is well documented and understood for one phase flow, there is still a substantial amount of research needed to make an accurate model for multi-phase flow.

This master thesis has focused on two main objectives. Firstly, to document and analyze a horizontal venturi behavior during wet gas conditions and its effect on a centrifugal compressor system. Secondly, explore the opportunity to make a digital model of the interactions between the venturi and the compressor.

To document the venturi behavior in wet gas the NTNU wet gas compressor laboratory has been used with a transparent venturi to gather data. Based on the data gathered, several notable interactions between the venturi and the compressor system were found and two distinct types of flow fields were documented in the divergent part of the venturi.

Firstly, a stable flow field with some back flow and secondly, an unstable flow field with accumulation of liquid in the divergent part of the venturi where the liquid periodical reenters the wet gas flow in large burst.

These venturi flow fields impact the compressor system creating larger volatility in the pressure of the flow -and the torque of the compressor. With the unstable flow field the Gas mass fraction (GMF) is constantly changing after the venturi and causes high spikes in torque when large amount of liquids reenter the wet gas flow. There was also documented a considerable higher compressor efficiency during the unstable flow field with low GMF at the venturi entrance.

Lastly, some concepts for a digital model utilizing torque measurements to determine the GMF and flow regime of the flow are discussed.

Abstract in Norwegian

Subsea våtgass kompressorer har blitt brukt for å øke utvinningen fra gassfelt siden 2015. Denne teknologien har et stort potensial for å øke produksjonen ytterligere og redusere kostnadene. Våtgass komprimering er fremdeles i en tidlig fase og krever mere utvikling for å gjøre systemene mer pålitelige, økonomiske og kommersielle.

Venturi er blitt brukt for å finne gjennomstrømning siden 1895 og er nå en av de vanligste metodene for gjennomstrømningsmålinger. Mens venturi-effekten er godt dokumentert og forstått for enfasestrømning, så kreves det fremdeles en del mer forskning for å lage en mer nøyaktig modell for flerfasestrømning.

Denne masteroppgaven har fokusert på to hovedmål. Først, å dokumentere og analysere oppførsel til en horisontal venturi med en våtgass gjennomstrømning og hvilke innvirkninger venturien har på et sentrifugalkompressorsystem. Mål to er å utforske muligheten til å lage en digital modell mellom venturien og kompressoren.

For å dokumentere venturiens oppførselen i våtgass er NTNU våtgasskompressorlaboratoriet blitt benyttet med en gjennomsiktig venturi for å samle inn data. Fra de innsamlede dataene ble det funnet flere bemerkelsesverdige interaksjoner mellom venturien og kompressorsystemet. To distinkte typer strømningsfelt ble dokumentert i den divergerende delen av venturien.

Det første strømningsfeltet er en stabil gjennomstrømning med noe tilbakestrømning. Det andre strømningsfeltet er et ustabilt strømningsfelt som akkumulerer væske i den divergerende delen av venturien og med periodiske mellomrom river med seg en del av den oppsamlede væsken.

Strømningsfeltene som blir generert av venturien påvirker kompressorsystemet og skaper mere støy i trykket og på dreiemomentet til kompressoren. Med den ustabile strømningen er gass masse fraksjonen (GMF) i konstant endring etter venturien og forårsaker høye hopp i dreiemomentet når store mengder væsker blir revet tilbake i gasstrømningen. Det er også en viss indikasjon på at den ustabile strømningen kan ha noe gunstig effekt på kompressoreffektiviteten ved lav GMF.

Til slutt diskuteres noen konsepter for en digital modell som bruker momentmålinger for å bestemme GMF og strømningsregime i en våt-gasstrøm.

Contents

List of Figures

Nomenclature

Symbols	Description	Unit
C	Discharge coefficient	-
D	Diameter	m
Fr	Densimetric Froude number	-
GMF	Gas mass fraction	-
g	Gravitation constant	$9.81\ m/s^2$
h	Enthalpy	J/kg
H	Head	J/kg
$\dot{m}$	Mass flow	kg/s
MW	Molecular weight	$kg/kmol$
n	Mole	mol
P	Pressure	N/m^2
Q	Volume flow	m^3/s
R_0	Gas constant	$8314\ J/(kmolK)$
Re	Reynolds number	-
RH	Relative humidity	-
s	Entropy	$J/kg \cdot K$
T	Temperature	K
TQ	Torque	N·m
u	Internal energy	J/kg
U	Velocity	m/s
V	Volume	m^3
X	Lockhart-Martinelli Parameter / Compressibilityl function X	-
Y	Compressibility function Y	-
Z	Compressibility factor Z	-

Greek

β	Venturi diameter ratio	-
δ	Density ratio	-
ϵ	Expansion factor	-
η	Efficiency	-
κ	Isentropic exponent	-
μ	Dynamic viscosity	$Pa \cdot s$
ν	Specific volume	m^3/kg
ρ	Density	kg/m^3
τ	Venturi pressure ratio	-
ϕ	Over reading correction factor	-
Ω	Rotational speed	rad/s

Abbreviations

BEP	Best efficiency point
EOS	Equation of state
FFT	Fast Fourier transform
FR	Flow regime
NTNU	Norwegian University of Science and Technology
PE	Dynamic pressure
SRK	Soave-Redlich-Kwong

Subscripts

1	Suction side
2	Discharge side
atm	Atmospheric
c	Compressor
DP	Differential pressure
g	Gas
l	Liquid
o	Orifice
P	Polytropic
s	Isentopic
v	Venturi
vt	Venturi throat
w	Water
ν	Specific volume

1 Introduction

In this chapter, the thesis background, scope, structure and some limitations with regard to the Covid-19 pandemic will be presented.

1.1 Background

The Paris agreement and the UN Sustainable Development Goals show the considerable attention the world has on energy and emissions. To reach these goals we need to continuously increase the efficiency of production by utilizing new innovative technologies and to search for more sustainable solutions. One of those new technologies is subsea wet gas compression for increased recovery rate by pressure boosting.

Subsea wet gas compression has large potential to extend production and to enable production at remote fields that without such technology would not be commercially viable. Even though subsea wet gas compression has great potential, there are still some challenges that need to be handled. Firstly, these systems need extraordinarily high reliability due to the immense work required to do necessary maintenance on the system. Secondly, that wet gas compression is at an early stage in its development and thus requires a lot of research to better understand the complex multi-phase interactions in such a system.

For optimal performance of subsea wet gas compressors, precise and continuous measurements are required for the control system. A common method for measuring flow rate is a venturi that utilizes the pressure drop over a decreased flow area to determine the flow rate. The venturi effect is well documented and understood for one phase flow. When used in wet gas flow the venturi inherently overestimates the flow rate due to two-phase interactions in the venturi [1]. Therefore, it is developed an ISO standard for overreading correction factor for wet gas flow in a venturi ISO/TR:11583 [2]. This standard is limited in its operational range and do not address several critical parameters, such as flow regime.

There is currently limited documentation and research into wet gas interactions in the venturi, other than the overreading corrections. Special interactions of interest is the generation of slugs from the venturi.

1.2 Scope of the thesis

The scope of the thesis is split into three parts which are derived from the master project description from page i.

Firstly, to establish relevant compressor performance characteristics. This will be done by analyzing data from the compressor system without the venturi and thus establish baseline performance for the compressor system. Then, subsequent tests can be compared with the base line performance.

Secondly, review and validate the venturi-tube behavior at wet gas conditions. Thirdly, establish and document a digital model of the interactions between the compressor and venturi-tube at different operating conditions. For this scope, the main

focus will be on the interactions between the venturi and compressor at wet gas conditions.

1.3 Thesis structure

The structure of this thesis is as follows.

- Chapter 1: Introduction - Introduces the reader to the background, scope and structure of the project work.
- Chapter 2: Compressor fundamentals - Provides fundamental knowledge of dynamic compressors, polytropic analysis, compressor characteristics and compressor control.
- Chapter 3: Venturi -& wet gas fundamentals - Provides fundamental knowledge of wet gas flow, venturi and wet gas corrections for venturi.
- Chapter 4: NTNU compressor laboratory & corresponding model - Describes the NTNU compressor laboratory, corresponding model made in Aspen HYSYS and the venturi.
- Chapter 5: Experimental cases - This chapter will describe the scope, procedure and execution of the 6 experimental cases with corresponding test matrices. Additional, some remarks regarding faults in the data logging system will be given.
- Chapter 6: Experimental results and discussion - This chapter will present the results with discussions concerning compressor performance and venturi wet gas interactions.
- Chapter 7: Digital model - This chapter will discuss several concepts with regards to a digital model for interactions between the compressor and venturi.
- Chapter 8: Conclusion - This chapter will give conclusions based on the results and will give recommendations for further work.

1.4 Limitations due to the Covid-19 pandemic

This thesis was written during the spring of 2020 during the Covid-19 pandemic. With Norwegian national guidelines closing universities, caused the access of laboratory to be severely limited. Due to this unfortunate situation all the data analyzed was collected before national guidelines was imposed, causing the data gathered to not entirely match between the baseline -and venturi cases. Additionally, only 2 flow regimes at the venturi entrance were documented. These limitations in the data will therefore reduce the reliability of some of the results.

2 Compressor fundamentals

This chapter will focus on basic of compression systems, operation and control of compressors.

2.1 Compressor

A compressor is a device used to increase pressure in compressible fluids. There are 2 main types, i.e. either positive displacement or dynamic compressors. Positive displacement compressors enclose the fluid and by decreasing the encapsulated volume, the pressure increases. Piston- and screw compressors are examples of positive displacement compressors. Dynamic compressors accelerate the fluid, and then convert the kinetic energy of the fluid to static pressure. Dynamic compressors can further be divided into axial- and centrifugal compressors [3]. The dynamic centrifugal compressors are widely used in industry and will be the main compressor type to be focused on in this thesis.

2.2 Centrifugal Compressor

A centrifugal compressor is composed of 1 or more compressor stages. Every stage consists of a rotating impeller and a diffuser. Figure 1 illustrates a single compressor stage and the subsequent text refers to Figure 1. The fluid enters the eye "c-a", then the fluid is guided into axial direction through the inducer part of the impeller. Next, the fluid is accelerated in the radial direction through the remaining part of the impeller. Throughout the whole impeller energy is transferred to the fluid in form of added pressure and kinetic energy. The fluid leaves the impeller "d-b" and enters the diffuser. The diffuser converts a greater part of the kinetic energy of the fluid into pressure energy. This is done by a gradually increase in area that slows down the fluid and thus in accordance with Bernoulli's principle the pressure will increase. The fluid is then collected by the collection scroll, and guided into the next compressor stage or the outlet of the compressor [4].

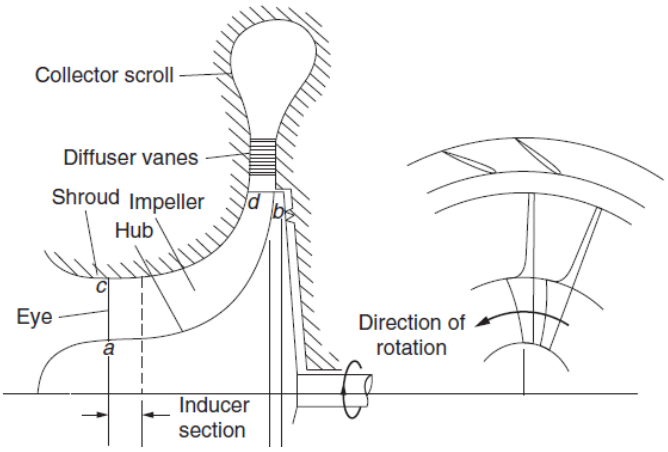

Figure 1: Centrifugal Compressor [4].

2.3 Equation of state (EOS)

Equation of state are the mathematical models used to correlate thermodynamic property interactions. However, at this time there exists no perfect EOS that fully correlates with the interactions of thermodynamic properties for real gases. Therefore, there are several EOS's, that provide different degrees of accuracy to real processes based on parameter range, specific fluid, specific processes, etc. The simplest EOS is the ideal gas law presented in Equation 2.1. The ideal gas law applies some simplifications, which include that there are no intermolecular attractions between gas molecules and that the particles represent no volume themselves. Due to these simplifications, the accuracy of the ideal gas law can deviate with several percent, compared to a real gas.

$$PV = nR_0T \tag{2.1}$$

To compare ideal gas law to real gases, compressibility factor (Z), defined in Equation 2.2, is used. When $Z \approx 1$ the gas behaves as an ideal gas. This is usual the case for monoatomic gases at low pressure. Hence, the larger the difference from $Z = 1$, the larger the deviation is between the real to the ideal gas. High deviation occurs near the critical point of the gas.

$$Z = \frac{PvMW}{R_0T} \tag{2.2}$$

Most other EOS's are based on the ideal gas law, combined with some sort of correction factors which are based on empirical data.

2.4 Polytropic head

To evaluate compressor performance against thermodynamic properties in an accurate way, a polytropic approach is required. The polytropic approach developed by Schultz [5], is used in compressor standards from both ASME and ISO. Figure 2 demonstrates the basic idea of a polytropic analysis and will be used for the following explanation. The isentropic head (H_s) is a compression process where no entropy is added to the system through the process, as depicted between "1" and "2_s" in the diagram. While the Total head (H) is the amount of energy used in the real system. From this we can find the isentropic efficiency (η_s) Equation 2.3.

$$\eta_s = \frac{H_s}{H} \tag{2.3}$$

This method does not take into account that the isentropic head in a real process follows the compression line from "1" to "2" in the figure. To make a better estimation of the real process a polytropic analysis is used where the polytropic process is divided into infinite numbers of steps along the compression between "1" and "2". The polytropic head (H_p) is the sum of the isentropic head (Δh_p) for all the steps along the compression line Equation 2.4.

$$H_P = \sum_{i=1}^{\infty} \Delta h_{P_i} \tag{2.4}$$

By definition the enthalpy h is Equation 2.5 and the derivative form of the enthalpy equation is Equation 2.6.

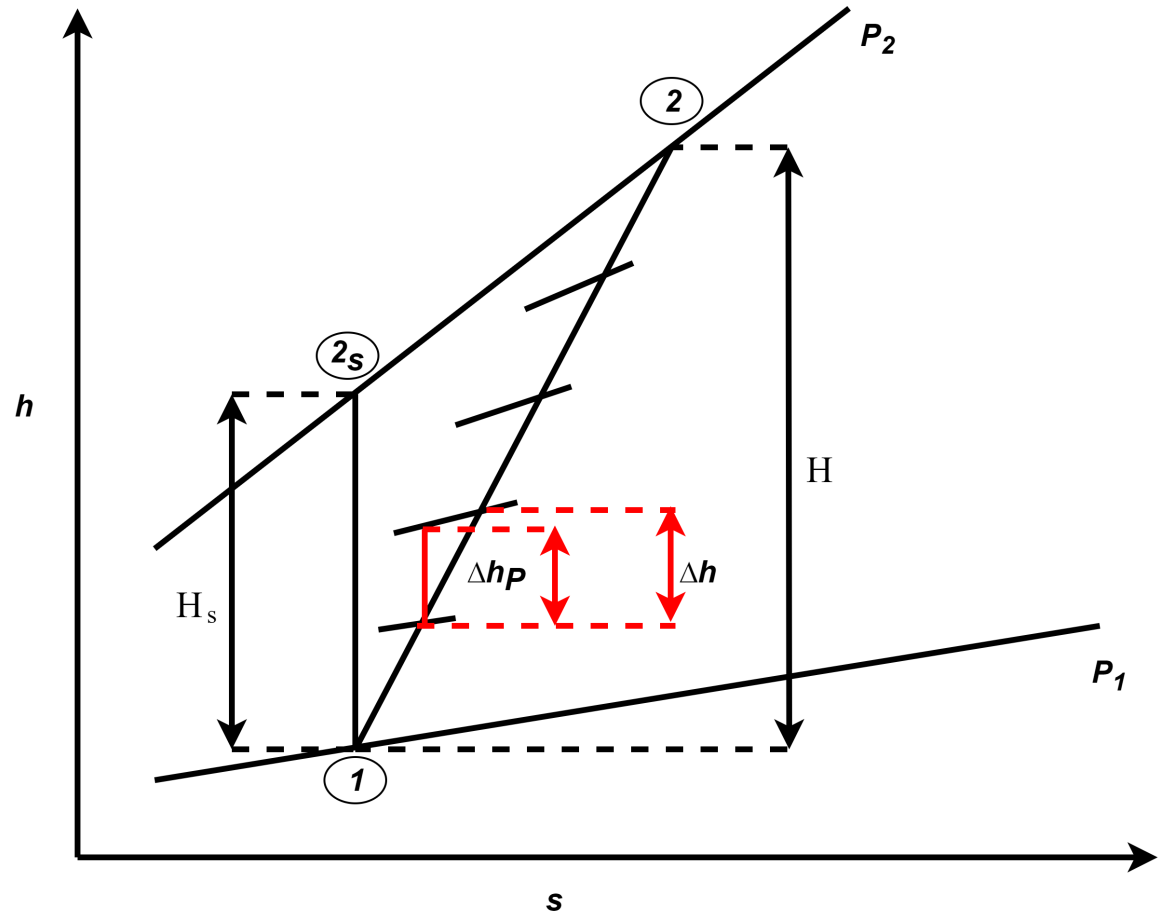

Figure 2: Polytropic process in an enthalpy entropy diagram

$$h = u + p\nu \tag{2.5}$$

$$dh = du + pd\nu + \nu dp \tag{2.6}$$

The derivative form of the internal energy (u), while neglecting minor energy terms as surface -and chemical energy, is given in Equation 2.7 .

$$du = Tds - pd\nu \tag{2.7}$$

Combining Equation 2.6 and 2.7 gives the infinitesimal change in enthalpy Equation 2.8.

$$dh = Tds + \nu dp \tag{2.8}$$

Considering that there is no change in entropy in an isotropic process i.e $Tds = 0$. Then the polytropic head can be expressed as the integral of the specific volume (ν), between "1" and "2" Equation 2.9. This integral was approximated by Schultz [5], by introducing 2 compressibility functions X Equation 2.10 -and Y Equation 2.11.

$$H_P = \int_1^2 \nu \, dP \approx \frac{n_\nu}{n_\nu - 1}[P_2 v_2 - P_1 v_1] \tag{2.9}$$

$$X = \frac{T}{\nu}\left(\frac{\partial \nu}{\partial T}\right)_P \tag{2.10}$$

$$Y = \frac{P}{\nu}\left(\frac{\partial \nu}{\partial P}\right)_T \tag{2.11}$$

Since the polytropic volume exponent (n_ν) changes along the compression curve an exact solution is hard to find and n_ν will be defined as an average between $n_{\nu,1}$ and $n_{\nu,2}$.

To take into account the variation of (n_ν) along the compression curve, a correction factor (f) was made by Schultz [5]. Combining Equation 2.2, Equation 2.9, Equation 2.12 and (f), an equation for polytropic head with only one parameter at the exit of the compressor can be made Equation 2.13.

$$Pv^{n_\nu} = Constant \tag{2.12}$$

$$H_P \approx f \frac{n_\nu}{n_\nu - 1} \frac{Z_1 R_0 T_1}{MW}\left[\left(\frac{P_2}{P_1}\right)^{\frac{n_\nu - 1}{n_\nu}} - 1\right] \tag{2.13}$$

When dividing the polytropic head by the total head, the polytropic efficiency is found, Equation 2.14. All later referrals of compressor efficiency in this work will refer to the polytropic efficiency.

$$\eta_p = \frac{H_p}{H} \tag{2.14}$$

2.5 Compressor Characteristics

Compressor characteristics, also known as compressor maps, are visual representations of the operational range and performance of the specific compressor. An example of a compressor map is illustrated in Figure 3. These maps usually have volumetric flow at the inlet as the x-axis versus discharge pressure, head or pressure ratio at the y-axis, and are further plotted for several rotational speeds, respectively. In this paper, head will be used as parameter for the y-axis. Nevertheless the general concepts are valid for the remaining y-axis parameters as well. These maps are valid for specific fluid properties as well as inlet temperature and pressure.

The best efficiency point (BEP) is set at the designed operational rotational speed, volume flow and head. Note that in the cases where the maps are shown in percent format, 100% refers to the design point and not to the maximum of the compressor. The operational range is limited by surge at low volume flow and choked at high volume flow. These limits are depicted by bold dashed line.

Surge occurs when a decrease in volume flow results in a decrease in outlet pressure. The pressure downstream of the compressor momentarily becomes higher than the outlet pressure, this results in a reversal of the flow direction. Further, this reversal in flow direction will increase the flow in the compressor, building up the pressure and

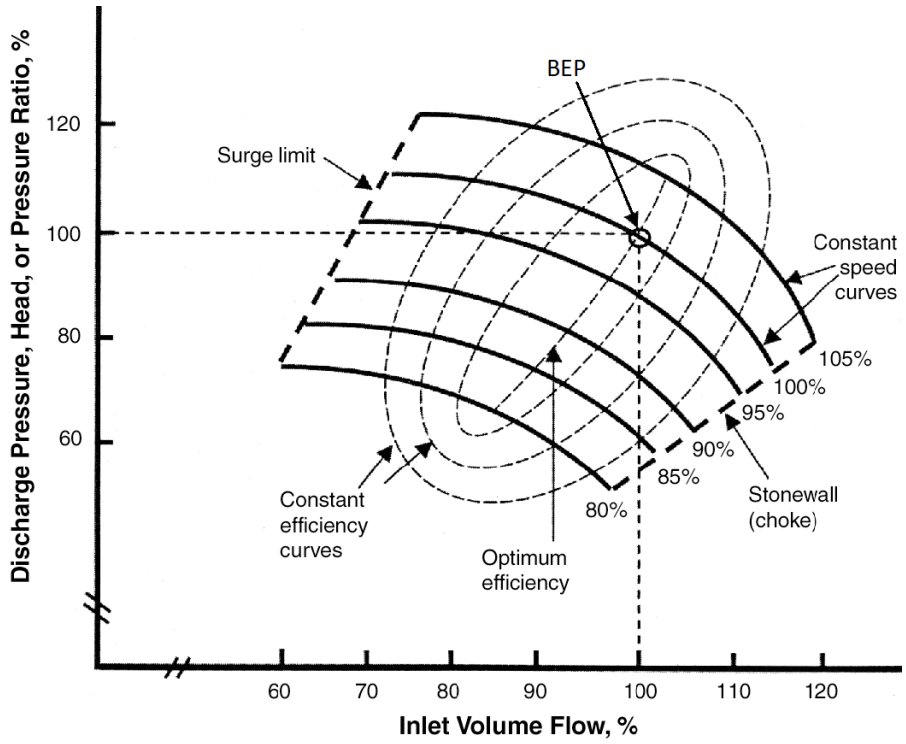

Figure 3: Centrifugal compressor performance map [6]

reverse the direction back to the original flow direction. These fluctuations can occur at a high frequency, and the resulting vibrations can rapidly damage the compressor [7]. The surge line will cross the rotational speed curves at the maximum value, due to that the point where a decrease in volume flow, starts to decrease the pressure.

Choking is mainly a limit set by the speed of sound in the compressor. It can be noted that contrary to stationary objects, that if the speed of sound is reached in the impeller, the volume flow can be increased by increasing the rotational speed. This is the reason that the choke line is not a vertical line. In contrary to surge, choking is not an immediate danger to the compressor. However, overheating can occur if the compressor chokes over a longer period of time.

The efficiency of the compressor is marked by thin dashed circles in the map and in the center of these circles are the optimum efficiency line that shows the highest efficiency at a given rotational speed.

2.6 Compressor Control

Compressors are used in various industrial processes that utilize the compressor in different ways. This leads to different parameters that the controller wants to regulate, where the most common are outlet pressure, mass flow and inlet volume flow. Thus, there are several ways to control the system including discharge throttling, suction throttling, recycling, speed variation and inlet guide vane angel variation [7]. Volume flow control with discharge throttling regulation will be used as a base in this work.

Figure 4 shows how discharge throttling changes the operating point on the com-

pressor characteristics. At point "A" discharge valve is 100% open, and it operates at choking condition, hence at maximum flow. When decreasing the opening on the discharge valve, the system resistance increases. This will force the compressor to build up higher pressure that subsequently decreases the volume flow. At constant rotational speed, the process will follow the speed curve, moving left in the diagram. When the discharge valve opening corresponds to a system resistance that coincides with the designed volume flow through the compressor, then the compressor works at its highest efficiency (depicted as point "B"). Decreasing the opening of the discharge valve even further,it will continue moving the operation point left along the speed curve until point "C" is reached. At this stage, the compressor can enter surge [7].

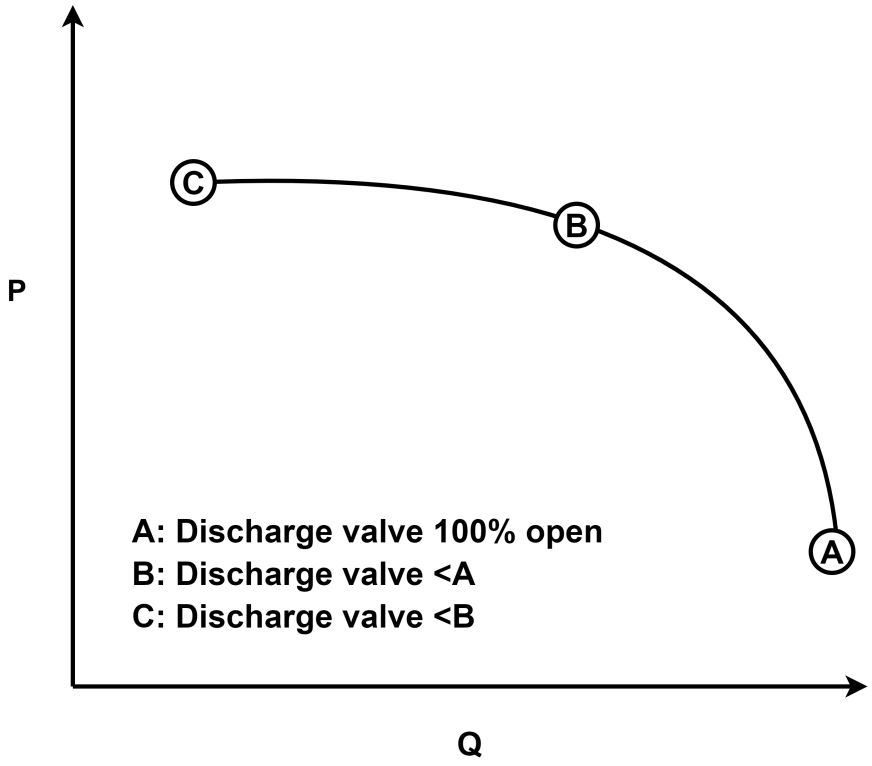

Figure 4: Discharge throttling effect along compressor characteristics. [6]

3 Venturi -& wet gas fundamentals

This chapter will begin with the basics of wet gas flow, followed by venturi fundamentals and end with wet gas interactions with venturi.

3.1 Wet gas fundamentals

There is no clear definition of wet gas [8]. In this thesis wet gas will use ISO/TR 11583 definition as being a two-phase flow of gas and liquid, consisting of 95% and higher volumetric gas flow [2].

A common way to describe the amounts of liquid in relation to gas in the fluid is by gas mass fraction (GMF) se equation 3.1.

$$GMF = \frac{\dot{m}_g}{\dot{m}_g + \dot{m}_l} \tag{3.1}$$

Another important parameter for wet gas flow is the density ratio (δ), which has a direct impact on phase separation.

$$\delta = \frac{\rho_g}{\rho_l} \tag{3.2}$$

There are two main stable flow regimes for wet gas flow in horizontal pipes, dispersed and stratified as depicted in Figure 5. In dispersed flow the liquid travels as droplets dispersed in the flow. With this flow regime the liquid droplets tend to behave similar to the gas, resulting in dispersed flow often can be analyzed as a one phase flow. Dispersed flow occurs when liquid is sprayed into the gas or after specific flow interactions that has a mixing effect. At high superficial gas velocity liquid tends to accumulate at the pipe wall, creating a liquid layer traveling with the wet gas flow. This kind of flow field is called annular flow and is considered as a dispersed flow for this thesis. Depending on the flow the majored liquid transport in annular flow can be either through the liquid film or by dispersed droplets.

With low superficial gas velocity, the liquid succumbs to gravitational forces and the wet gas segregates to a pure liquid phase at the bottom of the pipe, this flow is called stratified flow regime. During stratified flow the two phases has have a significant larger behavioral deference between them than during dispersed flow and is usually easiest to be analyzed as two separate flows.

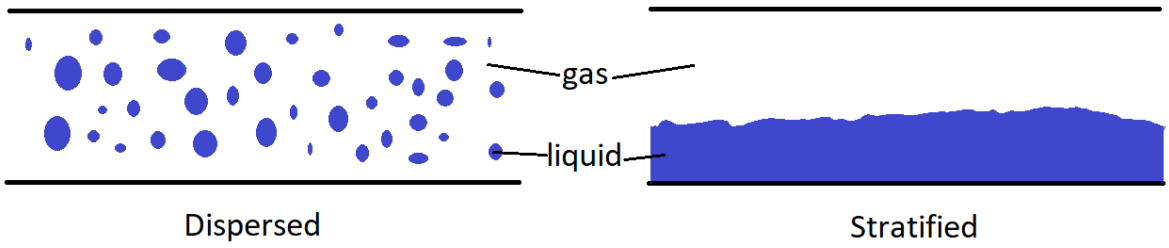

Figure 5: Flow regimes, with dispersed flow to the left and stratified flow to the right.

Flow regimes are created by a balance between stratifying -and mixing forces, where some of the critical parameters being inertia, being important for turbulence i.e mixing force and gravitational, viscous -and surface forces being important stratifying forces. Several non-dimensional groups has been created to relate the mixing -and stratifying forces to each other, with the most common being Reynolds number (Re) Equation 3.3 and Froude number (Fr) Equation 3.4 , the Froude number (Fr) will be further defined in 3.3.

$$Re = \frac{\rho u D}{\mu} = \frac{inertia}{viscus} \tag{3.3}$$

$$Fr = \frac{u^2}{gD} = \frac{inertia}{gravity} \tag{3.4}$$

3.2 Venturi dry gas fundamentals

A venturi is a device that is commonly used for flow rate measurements. The device utilizes Bernoulli's principle, that an increase in speed is linked to a decrease in static pressure, in order to determine the flow rate. For this thesis ISO 5167-4 [9] will be used as the basis for dry gas calculations. To determine the mass flow rate the Equation 3.5 is used.

$$\dot{m} = \frac{C}{\sqrt{1-\beta^4}} \epsilon \frac{\pi}{4} D_{vt}^2 \sqrt{2 \Delta P \rho_1} \tag{3.5}$$

"β" is the diameter ratio between the venturi inlet -and throat 3.6.

$$\beta = \frac{D_{vt}}{D_1} \tag{3.6}$$

"C" is the discharge coefficient that represents the difference between the actual venturi and an ideal venturi. Venturi with a machined convergent section has a discharge coefficient of 0.995 while used at dry gas condition [9].

"ϵ" is the expansion factor which is calculated by 3.7 where τ is the venturi pressure ratio between the venturi inlet -and throat 3.8. ϵ is only applicable if $\tau \geq 0.75$.

$$\epsilon = \sqrt{\left(\frac{\kappa\tau^{\frac{2}{\kappa}}}{\kappa-1}\right)\left(\frac{1-\beta^4}{1-\beta^4\tau^{\frac{2}{\kappa}}}\right)\left(\frac{1-\tau^{\frac{\kappa-1}{\kappa}}}{1-\tau}\right)} \tag{3.7}$$

$$\tau = \frac{P_{vt}}{P_1} \tag{3.8}$$

"ΔP" is the differential pressure between the venturi inlet -and throat 3.9.

$$\Delta P = P_1 - P_{vt} \tag{3.9}$$

3.3 Venturi wet gas fundamentals

When a venturi is used in wet gas condition the venturi inherently overestimates the gas flow rate. This is due to the liquid in the gas increases the differential pressure in the venturi. The degree of over-reading depends on several factors such as the GMF, where a decrease in GMF corresponds to an increase in over-reading, flow regime and geometric parameters [10].

A review of wet gas flow rate measurements by means of single-phase meters done by Munari et al. concluded that venturi was the most suitable device to measure wet gas flow [11]. Further, a review of the most common wet gas correlations done by Bjørner et al. [12] found that the Reader-Harris Graham correlation had the smallest deviation from experimental data. The Reader-Harris Graham correlation is the correlation used by ISO/TR 11583 [2] to correct ISO 5167 [9] for wet gas interaction regarding over-reading. The corrected gas mass flow calculation from ISO/TR 11583 is given in Equation 3.10.

$$\dot{m}_g = \frac{C}{\sqrt{1-\beta^4}}\epsilon\frac{\pi}{4}D_{vt}^2\frac{\sqrt{2\Delta P\rho_{1,g}}}{\phi} \tag{3.10}$$

The corrected mass flow calculation differs from the original, Equation 3.5, by 3 counts. Firstly, the mass flow that is calculated is only for the gas flow. Secondly, "C" is no longer a static number based on the venturi. While the venturi handles wet gas "C" is calculated by Equation 3.11. Lastly, the correction factor (ϕ) is introduced.

$$C = 1 - 0.0463e^{\left(-0.05\frac{Fr}{\beta^{2.5}}\right)} * min\left[1, \sqrt{\frac{X}{0.016}}\right] \tag{3.11}$$

The Lockhart-Martinelli Parameter (X) correlates the phase -and density ratio of the gas, see Equation 3.12.

$$X = \left(\frac{\dot{m}_l}{\dot{m}_g}\right)\sqrt{\delta_1} \tag{3.12}$$

The Froude number is a common multi-phase parameters that is an form of ratio between inertial and gravitational forces, where inertial forces is inclined to mix phases and gravity is inclined to separate phases. Further, can the Froude number be modified to account for density difference between the phases resulting in the densimetric Froude number given in Equation 3.13.

$$Fr = \frac{4\dot{m}_g}{\rho_g \pi D^2 \sqrt{gD}}\sqrt{\frac{\rho_g}{\rho_l - \rho_g}} \tag{3.13}$$

The over-reading correction factor (ϕ) is given in Equation 3.14. Where "n" is a parameter based on experimental data.

$$\phi = \sqrt{1 + X(\delta_1^{-n} + \delta_1^n) + X^2} \tag{3.14}$$

ISO/TR 11583 has several limitations in range of application including that, the density ratio $\delta \geq 0.02$, Lockhart-Martinelli Parameter $X \leq 0.3$ and the Froude number over the diameter ratio $Fr/\beta^{2.5} \geq 3$. The standard does not consider the flow regime and specifically states that differences in flow regime can produce widely differences in the mass flow estimation. It can also be noted that the standard specifically states that it is not intended for the oil -and gas industry.

4 NTNU compressor laboratory & corresponding HYSYS model

In this chapter, the NTNU compressor laboratory -and corresponding model in Aspen HYSYS will be described.

4.1 NTNU compressor laboratory

The NTNU compressor laboratory is shown in Figure 6. It is more formally known as "Wet Gas Compressor and Multiphase Boosting Test Facility", and the laboratory's objectives are to validate dry -and wet gas compression systems and to develop in depth knowledge of fundamental mechanisms of wet gas compression behavior.

The compression system uses a single stage, low-pressure centrifugal compressor. It utilizes ambient air and water as working fluids in an open loop. The compressor is driven by a 450kW variable-speed drive electrical motor with a maximum rotational speed of 11 000 rpm. Figure 7 shows the P&ID of the compressor system.

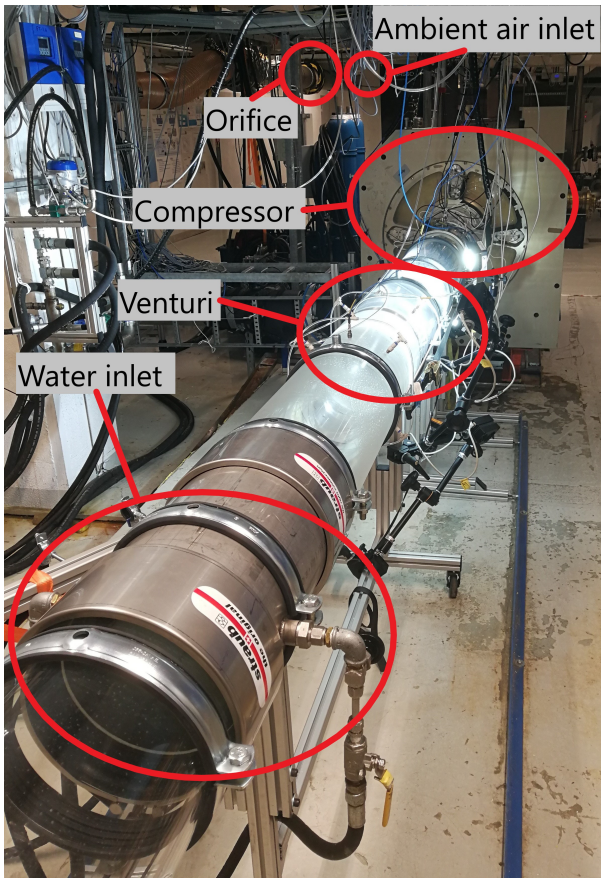

Figure 6: NTNU compressor laboratory.

Previous experiments have shown that the compression rig, with its low pressure ratio, gives comparable performance behavior to high pressure hydrocarbon systems [13]. The compressor laboratory instrument -and compression setup is validated in accordance with ASME PTC-10 [14]. Further measurement accuracy and operational range of the system be can found in Appendix A. A thorough description of the compressor laboratory can be found in "INTEGRATED WET GAS COMPRESSOR TEST FACILITY" by Hundseide et al. [13].

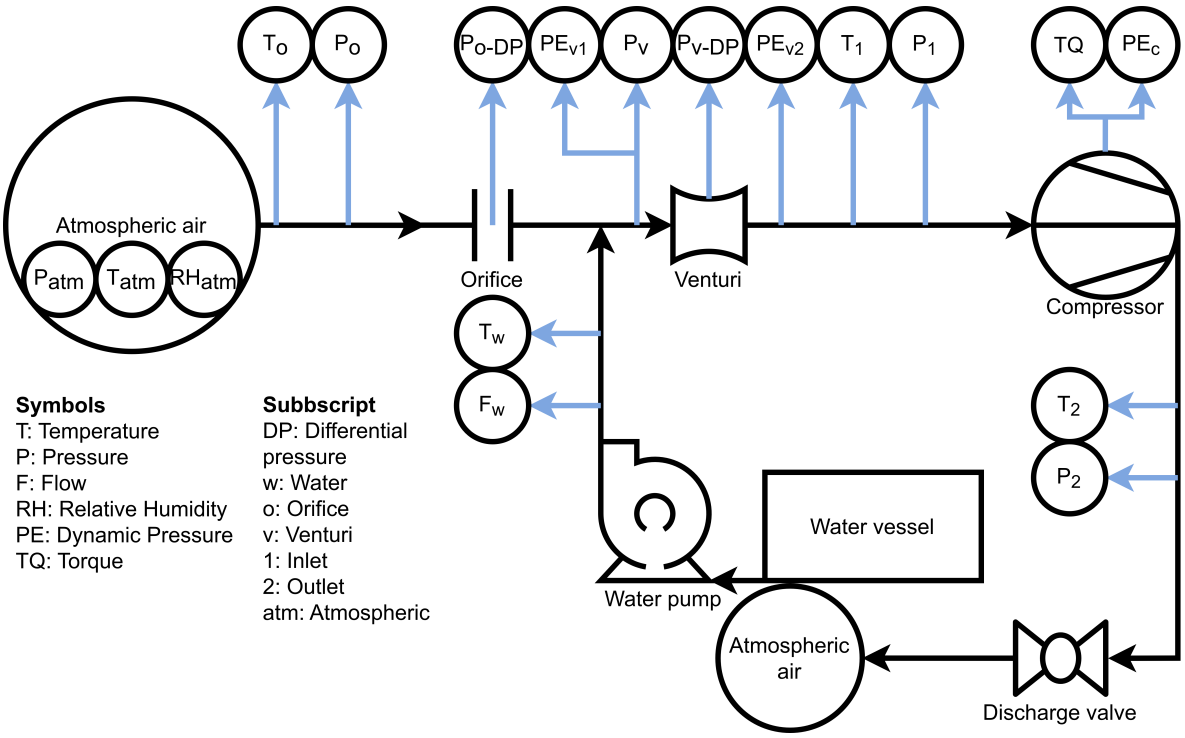

Figure 7: NTNU Compressor laboratory P&ID

4.2 Model inn HYSYS

The model imitating the compressor laboratory is presented in Figure 8 which will be used in the following explanation. This model is made in Aspen HYSYS by the thesis writer and uses Soave-Redlich-Kwong (SRK) as EOS. SRK was chosen as EOS due to its use in other projects regarding the compressor laboratory with wet gas conditions. "Saturated water" and "Dry air" are theoretical streams used by the "Saturater" to control the humidity in the Ambient air. The "Ambient air" simulates the ambient air that is the source of fluid for the compressor. Measurements of temperature, pressure and humidity are available for ambient air in the compressor laboratory. The calculations for the mass flow of "Ambient air" are done in accordance with ISO 5167-2 [9] and uses the measurements from the orifice. The valve "Pressure drop before compressor" simulates the reduction in pressure from ambient to the entrance of the compressor as a result of the suction from the compressor. "Dry suction air" is the state of the gas before water is injected into the gas stream. "Water inlet" represents the water that will be injected into the gas stream. "MIX-100" serves as the injection stage. Note that this HYSYS model will merely use energy and mass balances to calculate values, and will therefore not consider effects from the flow regimes or flow field specific parameters.

"1" is at the entrance of the compressor. At this stage, pressure is defined from the pressure measurements at the inlet of the compressor. The temperature is defined by temperature measurements from the orifice. This is due to the phases in the wet gas not necessarily has reached its temperature equilibrium which may result in unreliable temperature measurements at the compressor inlet. The compressor uses the torque

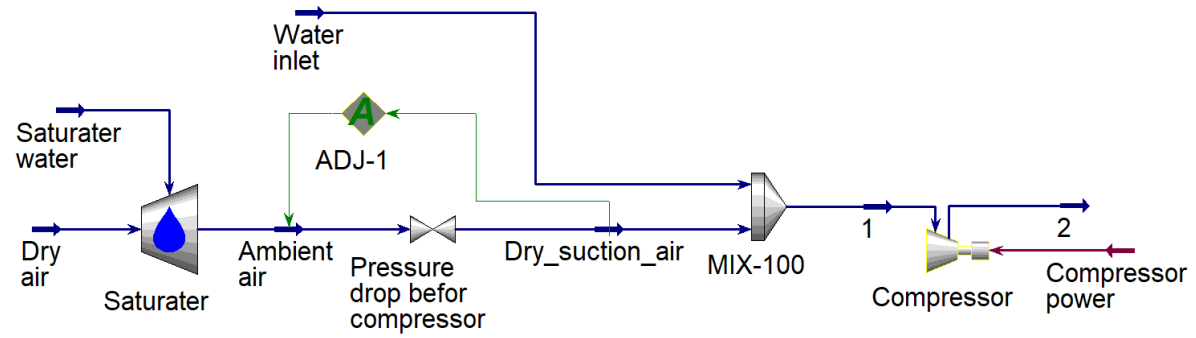

Figure 8: Model made in HYSYS

and rotational speed to define the energy added to the system. "2" is located after the exit of the compressor and uses pressure measurements from the compressor outlet. The model can also use the temperature measurements at the compressor outlet instead of the torque and rotational speed used in the compressor to define the model. Torque and rotational speed are used due to they are considered as more reliable measurements, especially during wet gas conditions.

4.3 The venturi

The venturi depicted in Figure 9 is made by machined transparent PMMA and is constructed in accordance to ISO 5167-4 [9] with some wet gas considerations regarding the convergent angle. The dimensions of the venturi are given in Table 1. It can be noted that the venturi uses 4 pressure tappings for each pressure measurement that is in accordance to ISO 5167-4. This means that the correction for wet gas, of using a single pressure tapping from ISO/TR 11583 [2], is not used.

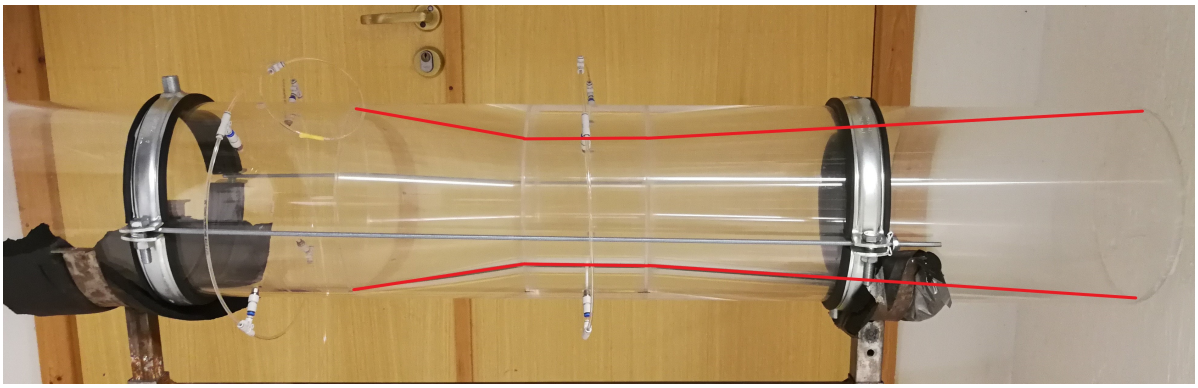

Figure 9: The venturi

The venturi is horizontal mounted and Figure 10 shows where in the compressor system it is inserted. To generate two different flow regimes to the inlet of the venturi the water injection is added at different locations for the different tests. To generate a semi-dispersed flow the water injections is mounted in a 30° down wards from the center line 1090 mm from the venturi inlet. To generate a more stratified flow the water injection is moved to 3970 mm from the venturi inlet. The longer travel distance lets the flow settle to its expected stratified flow regime.

Table 1: Venturi dimensions

Parameter	Quantity
Diameter ratio (β)	0.652
Inner pipe diameter	230 mm
Throat diameter	150 mm
Convergent angle	20.4°
Divergent angle	7.4°
Pressure tapping diameter	4.2 mm

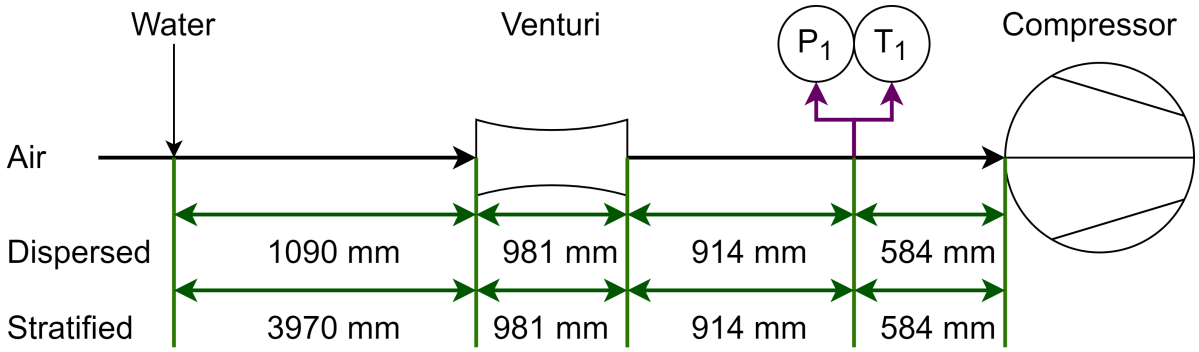

Figure 10: locations of the venturi in the system

5 Experimental cases

This chapter will focus on the scope, procedure and execution of the cases.

5.1 Experimental cases

1. Validation of the digital model.
2. Establish performance characteristics for the compressor without the venturi.
3. Identifying points of interest in dispersed inlet regime.
4. Stability testing points of interest in dispersed inlet regime.
5. Identifying points of interest in stratified inlet regime.
6. Stability testing points of interest in stratified inlet regime.

5.2 Case 1: Validation of the digital model

5.2.1 Scope

This case is a collaborative experiment planed by the 4 students currently utilizing the NTNU compressor laboratory for their master thesis.

The first case has two main purposes. Firstly, to validate the models made in Aspen HYSYS. And, secondly, to increase the understanding and knowledge of the compressor system functionality, instrumentation, procedures and the computation of the data.

5.2.2 Procedure

This case is split into tree subcases, operational range of 9 000 rpm, 11 000 rpm and stability of 9 000 rpm at best efficiency point (BEP), respectively named Case 1.1, Case 1.2 and 1.3. The key parameters for these cases are presented in Table 2.

Case: 1.1 is performed at 9 000 rpm. The discharge valve starts at 100% opening and is gradually closed to an opening of 25% over a 1-minute-period. The valve opening at 25% is held for 5 seconds and then the valve is returned to 100% opening over a 1-minute-period. Finally, this process is repeated once more. The data sampling rate is set to 2 Hz which is the default sampling rate for the system.

Case: 1.2 is performed at 11 000 rpm. The discharge valve starts at 100% opening and is gradually closed to an opening of 25% over a 10-second-period, where the opening of 25% is held for 1 second before the opening is returned to 100% over a 10-second-period. The data sampling rate is set to 20 000 Hz which is the fastest measuring speed for the system. The faster opening and closing of the valve compared to case.1.1 is done principally to avoid an excessively large data file due to the high-speed sampling. Both case 1.1 -and 1.2 will mainly be used to gain familiarity with the system.

Case: 1.3 is stability testing at 9 000 rpm while the discharge valve is set to 54% which corresponds to BEP for the compressor. Due to the compressor using the air in the laboratory as working fluid, the inlet temperature to the compressor will increase until an equilibrium between heat loss from the compressor system and heat loss of the room is reach. This takes several hours and modified stability criteria from PTC-10 [14] is used in order to define the system as stable. PTC-10 is designed for

commercial compressor system with a much higher pressure ratio than what the test system uses. Thus, the stability criteria from PTC-10 is not strict enough for temperature stabilization of the system. The temperature stabilization criteria were changed from a maximum difference of 0.5% °R over 15 minutes as the inlet temperature to a difference of 0.2 C° over 15 minutes, while the remaining criteria from PTC-10 was retained. The Procedure for case 1.3 can be found in Appendix B.1.

Table 2: Test matrix Case 1

Parameter	Case 1.1	Case 1.2	Case 1.3	Unit
Rotational speed	9 000	11 000	9 000	rpm
GMF	1	1	1	-
Valve position	100-25	100-25	54 (BEP)	%
Sampling interval	2	20 000	2	Hz

5.2.3 Execution and observation

Some unusual phenomena were observed with regard to the data from several instruments in the laboratory. These phenomena occurred in several of the succeeding cases and will be discussed later in section 5.9.

5.3 Case 2: Compressor characteristics / Base performance

5.3.1 Scope

This case is a collaborative experiment planed by the 4 students currently utilizing the NTNU compressor laboratory for their master thesis.

The main goal of this case is to document the baseline performance of the compressor system. This is performed for 2 reasons. Firstly, to generate data that can be used to compare the data collected after the venturi is added to the system. Secondly, to complete the first task of the master project "Establish relevant compressor performance characteristics" as stated on page i.

5.3.2 Procedure

The test matrix for case 2 is given in Table 3. For this case there will be used two separate procedures. One for stability testing with GMF 1 and one for all other GMFs. For testing with GMF 1 the same stability criteria used in case 1.3 5.2.2 will be used. When there are liquids in the gas, i.e when the GMF is not 1, the compressor system reaches stability fast. Hence, the stability criteria for the system during wet gas conditions are changed to a specific period of test time decided as 5 minutes. The Procedure for the case can be found in Appendix B.2. Notable, the test with GMF 1 will use the procedure for case 1.3 Appendix B.1.

5.4 Case 3: Dispersed GMF variation

5.4.1 Scope

The main object of this test is to identify specific GMFs of interest from visual observations of the flow behavior in the venturi.

Table 3: Test matrix Case 2

Parameter	Case 2	Unit
Rotational speed	9 000	rpm
GMF	1/ 0.98/ 0.90/ 0.75	-
Valve position	100/ 75/ 54/ 42/ 30	%
Sampling interval	2	Hz

5.4.2 Procedure

The venturi is mounted to the system as described in 4.3. The compressor system will operate at 9 000 rpm and with the discharge valve sett to 54%. The amount of water injected into the stream will be slowly and stepwise changed between GMF of 1 and 0.66. The flow behavior will be analyzed from visual observations to identify specific GMFs of interest for stability testing in the next case.

5.4.3 Execution and observation

Figure 11 shows the pipe section immediately before the venturi. The image shows that a large part of the liquids travel dispersed in the gas and a small stratified liquid region at the bottom part of the pipe.

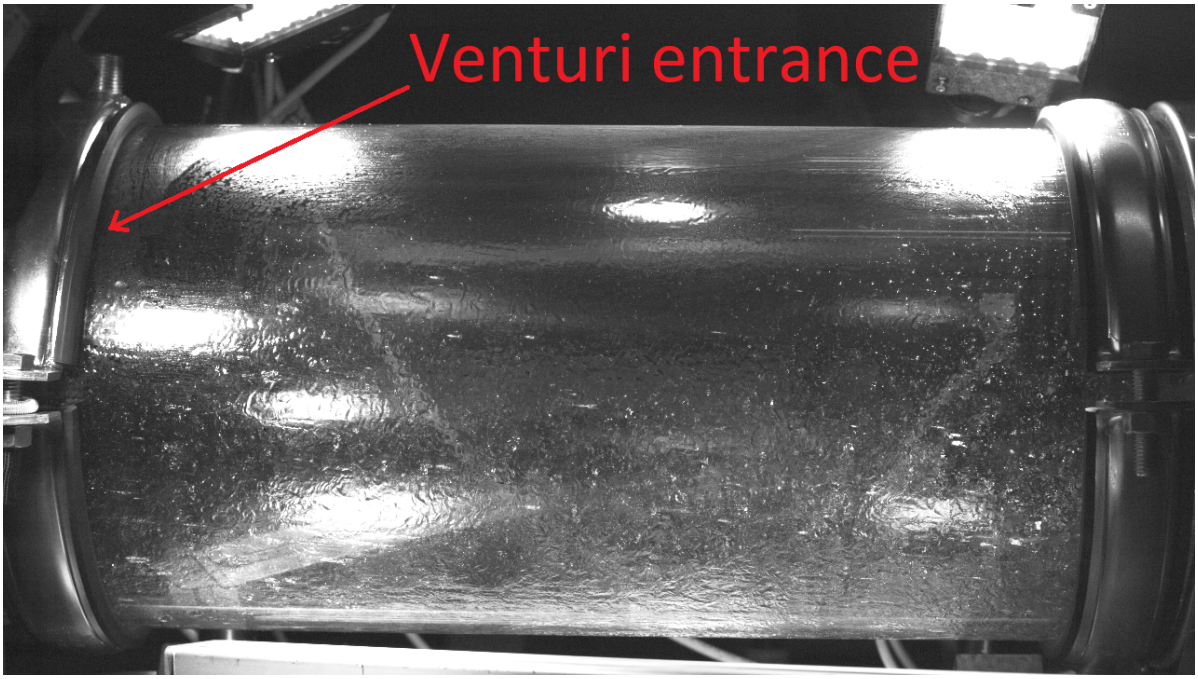

Figure 11: Flow regime at venturi entrance at GMF 0.85 for dispersed case.

5.5 Case 4: Dispersed points of interest

5.5.1 Scope

The main objectives of this case is to generate data that can be used to determine wet gas impact on the venturi and the venturi's impact on the compressor system.

5.5.2 Procedure

The test matrix for case 2 is given in Table 4. It can take several minutes for the flow behavior from the venturi to be fully established. To ensure that the flow is fully developed a period of 15 minutes is added between setting the GMF and logging the data. A sampling interval of 20 000 Hz is chosen to be able to perform fast Fourier transform (FFT) analysis for high frequencies. A high-speed camera is applied in order to visualize the flow behavior for the different tests. The Procedure for the case can be found in Appendix B.3.

Table 4: Test matrix Case 4

Parameter	Case 4	Unit
Rotational speed	9 000	rpm
GMF	1/ 0.98/ 0.90/ 0.88/ 0.87/ 0.84/ 0.78	-
Valve position	54	%
Sampling interval	20 000	Hz

5.5.3 Execution and observation

The venturi generates flow behavior with more volatility in pressure and torque, this will be discussed further in 6.3.1. With these fluctuating parameters the flow will not reach stability in accordance with PTC 10.

5.6 Case 5: Stratified GMF variation

5.6.1 Scope

The main object of this test is to identify specific GMFs of interest from visual observations of the flow behavior in the venturi.

5.6.2 Procedure

The venturi is mounted to the system as described in 4.3. The compressor system will operate at 9 000 rpm and with the discharge valve sett to 54%. The amount of water injected into the stream will be slowly and stepwise changed between GMF of 1 and 0.66. The flow behavior will be analyzed from visual observations to identify specific GMFs of interest for stability testing in the next case.

5.6.3 Execution and observation

The flow entering the venturi mostly stratified flow as depicted in figure 12. There is still some dispersed flow, which is hard to see from a still image.

5.7 Case 6: Stratified points of interest

5.7.1 Scope

The main objectives of this case is to generate data that can be used to determine wet gas impact on the venturi and the venturi's impact on the compressor system.

5.7.2 Procedure

The test matrix for case 2 is given in Table 5. The procedure for this case will be the same as for case 4 described in 5.5.2, except that the sampling time is changed to 1

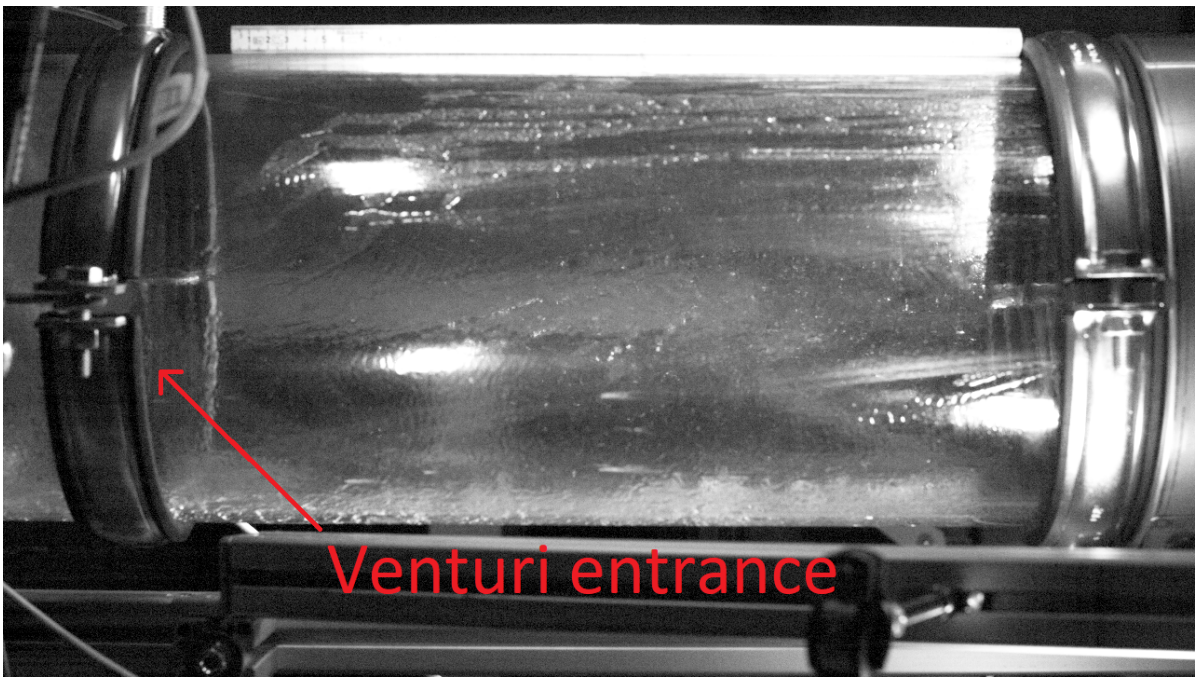

Figure 12: Flow regime at venturi entrance at GMF 0.85 for stratified case.

minute. This is changed because 2 minutes sampling time makes excessively large data files. The Procedure for the case can be found in Appendix B.4.

Table 5: Test matrix Case 6

Parameter	Case 6	Unit
Rotational speed	9 000	rpm
GMF	1/ 0.98/ 0.95/ 0.90/ 0.84 / 0.78	-
Valve position	54	%
Sampling interval	20 000	Hz

5.8 Still test

5.8.1 Scope

The still test is performed to ensure measurement devices operates at a correct manner, in which there is no interference on the data collecting system. Additionally, the still test generates data that can be used to compare and correct the operational data.

5.8.2 Procedure

The still test is performed as the first test every new day the compressor system is used for testing. The drive to the compressor and the hydraulic system is turned on before the test is initiated, to ensure that there is no interference from these devices upon the measurement system. The test is done before the compressor is started.

5.8.3 Execution and observation

Specific operational measurement data that was corrected utilizing this test was the differential pressure over the orifice (PT-3.1), which at standstill should be close to zero, but measured around 1 millibar. The specific value of the day was subtracted from the operational data. This correction of the mass flow of air caused by this subtraction was less than 2% from mass flow calculated without the subtraction.

Four sensors each measured the pressure and temperature before and after the compressor. In accordance with PTC-10, sensor that had a significant deviation from the others was excluded from the analysis.

5.9 Faults in data logging system

During the experimental campaign disturbances upon several measurements were observed. Figure 13 illustrate some of these disturbances. On the left-hand side of the figure the outlet temperature from the compressor shows that in some instances the measurement from a given instrument jumps to another measurement or to zero. On the right-hand side, the inlet pressure of the compressor exhibits periodic higher values. Several other instruments show similar tendencies which occur at the same time for all the instruments.

These interferences were new to the compressor laboratory and it is not known what caused them. During the data processing the distinct periods with interference was omitted.

However, these interferences in the data logging system made the data and thereby the results less reliable.

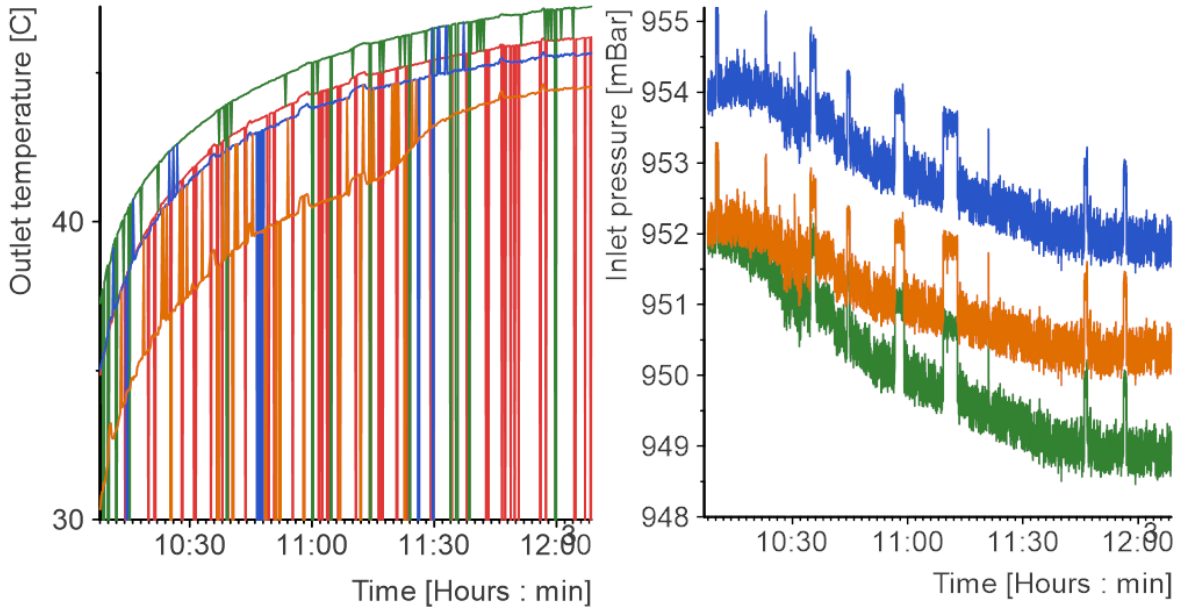

Figure 13: Temperature and pressure measurements showing disturbances during data collection.

5.10 Summary

In this chapter the different cases in the thesis are explained. The various cases consist of the first case which validate the accuracy of the model made in HYSYS 8. Then, the second case establish the base line performance of the compressor system before the venturi is added. Lastly, case 3-6 consist of investigations into how the venturi interacts with the compressor system.

6 Experimental results and discussion

This chapter will focus on the results gathered from the experimental campaign and the discussion of those results. The results will be presented in the following order. Firstly, validation of the HYSYS model followed by the compressor performance characteristics for the original system without the venturi. Finally, the results from the venturi experiments will be presented.

6.1 Validation of the digital model

To validate the HYSYS model described in 4.2, the data from case: 1.3 described in 5.2.2 are used. From the gathered data shown in Appendix C, there are two separate ways to define the energy added to the system.

The first method is to measure the direct energy added via torque measurements (TQ). The torque will provide a slightly higher energy than the actual energy added to the flow due to frictional losses. Earlier works on this compressor have shown that this loss by friction is approximately 70W. Compared to the total power consumption of the various tests conducted, that have at least a consumption of 28 KW, indicates that the frictional losses has no significant impact on the results.

The second method is to use the temperature at the outlet of the compressor, which together with the outlet pressure gives the enthalpy at outlet. Due to changes in the flow, even with the tolerances given for the test, the temperature measurements will trail behind the actual temperature of the flow and additionally some heat loss is expected to the compressor and the metal piping of the outlet.

The torque is chosen to define the model due to its more reliable measurements. Especially in wet gas flow where the temperature of the liquid and the gas can differ. While using the torque measurements the HYSYS model solves the temperature to be 47.81°C. The outlet temperature measured by 4 separate temperature sensors are shown in figure 14. Some of the disturbances of the measurements that was discussed in 5.9 are clearly visible but assumed to not have significant impact the results.

Only the last 15 minutes of the graph is within the pre-determined stability described in 5.2.2 with T_{2_2} measuring the highest temperature at 47.21°C. T_{2_4} show a significant difference of the data with respect to both the numerical values and the shape of the graph. It is therefore excluded from the remaining calculations in accordance with ASME PTC 10 guidelines for data treatment. After T_{2_4} is exclusion, T_{2_3} has the lowest value at the last measuring point at 45.65°C. The average of the measurements resulted in an outlet temperature of 46.35°C, which is 1.46°C lower than the temperature calculated by the model. Thus, this difference in temperature gives a difference of 5.25 percentage points in polytropic efficiency. This may have a significant impact on the results and can indicate fault in the measurement system or the model.

For two-phase flow, the phases can have different temperature which makes the temperature measurement less reliable for wet gas flow. Therefore, the temperature

data used in the model is obtained from sensor T_o temperature at the orifice instead for T_1 (see figure 7 in section 4.1 for placement of measurement devices). Based on the pressure drop from T_o to T_1, the temperature should differ by about 0.02°C for the dry gas cases if heat loss is not considered. The data gathered from the dry gas cases demonstrated that the differences from these sensors are as high as 1.3°C, which may have a large impact on the magnitude of the numerical values in the results. For this thesis, the differences of the cases are the most critical, and therefore it appeared more suitable to define the model from T_o rather than from T_1. This is due to that the changes in GMF will have an large impact on T_1 measurements.

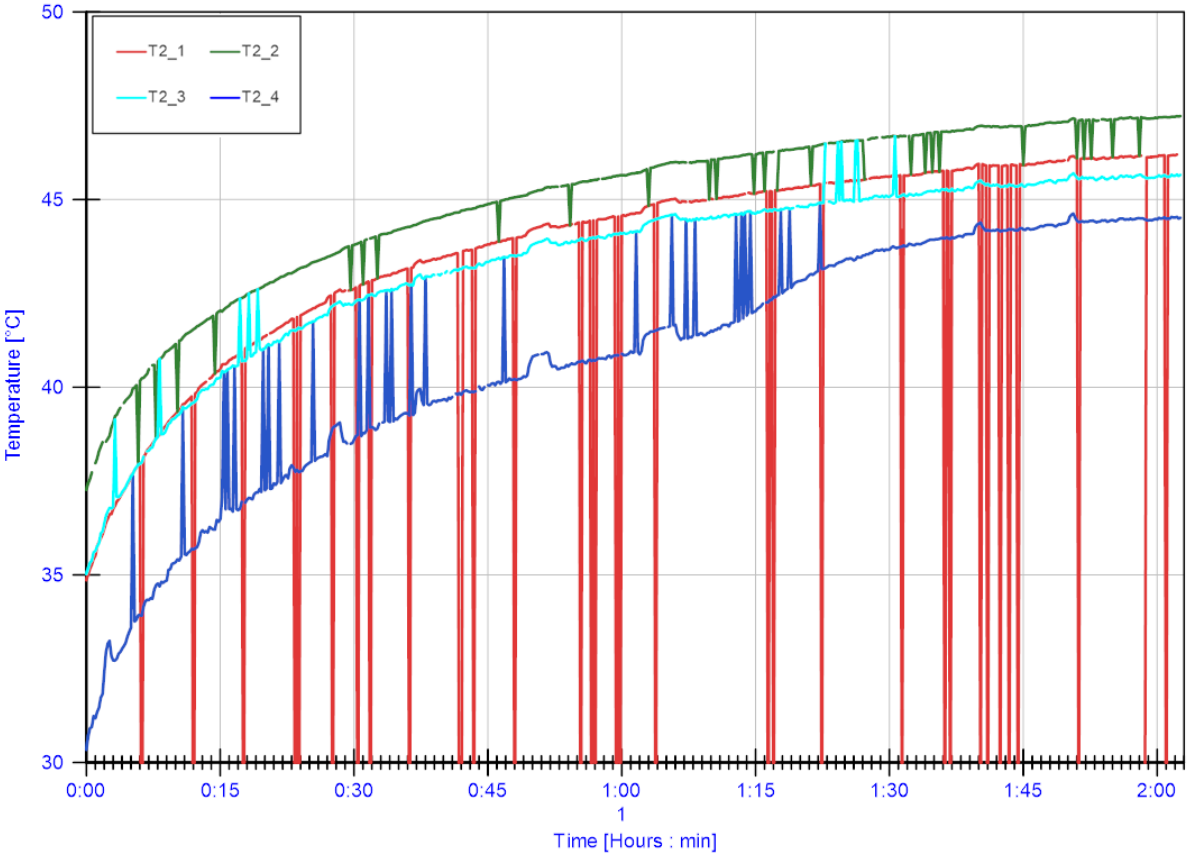

Figure 14: Temperature measurements for the 4 T_2 sensors for the dry gas verification case.

6.2 Compressor performance characteristics

This section will focus on the on the base line compressor system without venturi. The data from case 2 described in 5.3 will be utilized and case 1.3 will be used for the basis of normalization of the results.

6.2.1 Polytropic head

The polytropic head (H_P) of the compressor system for GMF 1/ 0.98/ 0.90/ 0.75 is plotted against the inlet volume flow rate in figure 15. From the definition of H_P equation 2.13, H_P is equivalent to the difference in specific volume. Due to the incompressibility of water, a reduction of H_P is expected as a result to a decrease of GMF. Figure

15 shows a distinct reduction in H_P and an offset of the operational range towards lower volume flows with lower GMF.

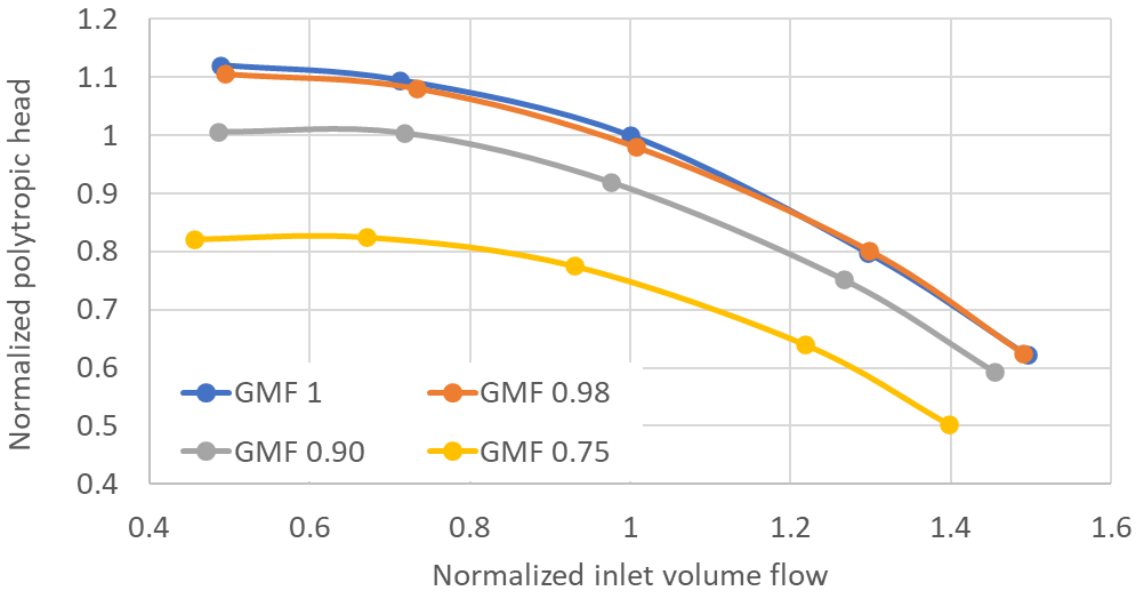

Figure 15: Normalized polytropic head for the compressor without the venturi.

6.2.2 Polytropic efficiency

The polytropic efficiency (η_P) of the compressor system for GMF 1/ 0.98/ 0.90/ 0.75 is plotted against the inlet volume flow rate in figure 16. The figure shows a clear decrease of η_P with reduced GMF. At GMF 0.75 there is a distinct alteration of the shape of the characteristic. Similar alterations of the characteristics for low GMF has been documented by Bakken, M at al. [15]. The reduction of η_P can be contributed to multi-phase interaction in the compressor and change in geometry in the compressor due to formation of a liquid film on the components. The data shows a reduction of T_2 with the reduced η_P. Following a reduction of η_P an increase of T_2 is expected for normal dry operations. This increase in temperature is counteracted by the addition of liquid with substantial higher heat capacity, and the occurrence of mass transfer between the phases.

6.2.3 Pressure ratio

The pressure ratios of GMF 1/ 0.98/ 0.90/ 0.75 is plotted against the inlet volume flow rate in figure 17. The figure shows that GMF 1 has a lower pressure ratio at low and medium inlet flow and that GMF 0.75 has the lowest ratio at the highest flow rate. GMF 0.75 as the lowest GMF has the second lowest pressure ratio at low and medium inlet flow. There is a difference in the shape of the pressure ratio curves, where lower GMF tends to have a sharper decline at the higher volume flows. The difference in pressure ratio in wet gas can be explained by multi-phase behavior in the compressor like liquids not dispersing in the compressor volute or swirling of liquids as documented by Bakken et al. [16]

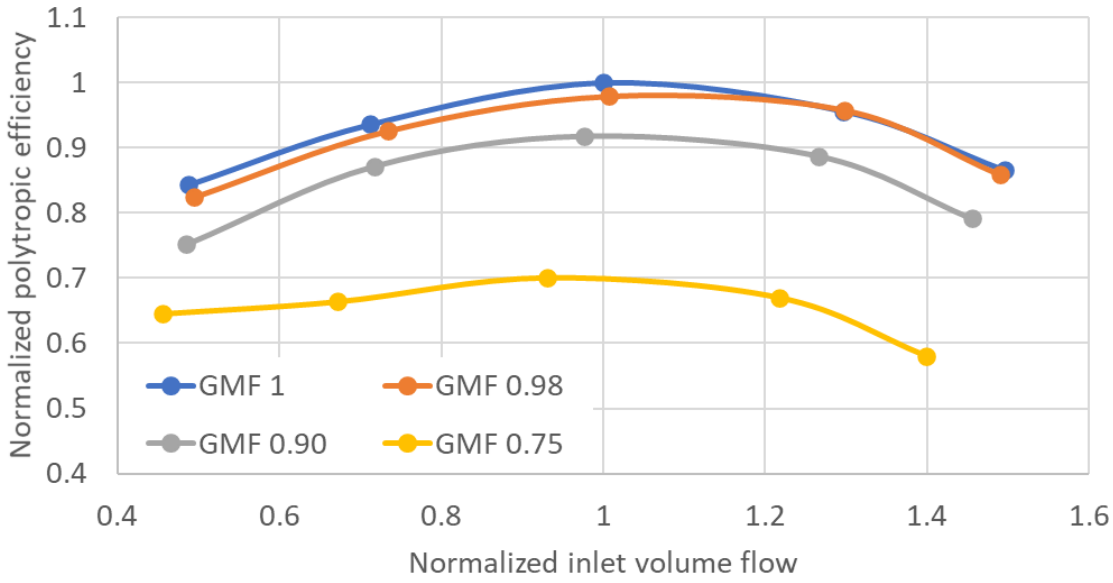

Figure 16: Normalized polytropic efficiency for the compressor without venturi

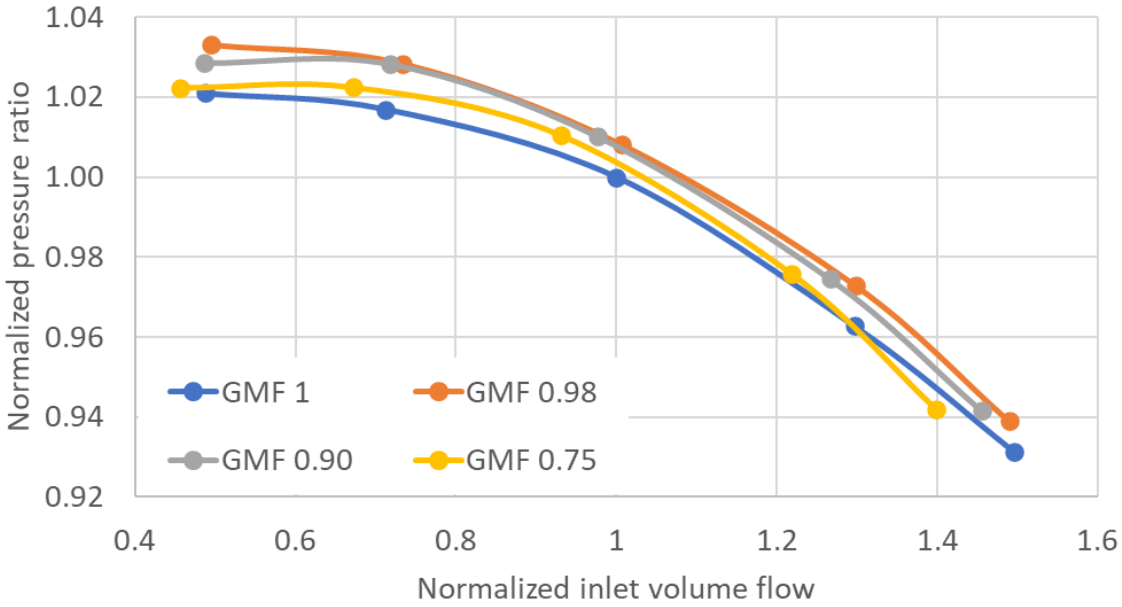

Figure 17: Normalized pressure ratio for the compressor without venturi

6.3 Venturi interactions on the compressor system

This section will describe the findings regarding the venturi, showing the most prominent findings at start. The data from case 3-6 described in 5.4 will be used for these results.

6.3.1 Liquid swirl

For horizontal mounted venturi, within a specific range of flow conditions a backward flow occurs at the lower part in the divergent venturi section at multi-phase flow. This backward flow can generate two different kinds flow fields. Firstly, the backward flow can generate small stable swirls as illustrated in Figure 18. This flow field generates small pulsations of the flow that can be noticed by several of the measurement devices in form of higher variations between each measurement point. This will be discussed later for each separate parameter. This flow field seems to occur at high GMF or low flow speed or with a more dispersed flow regime. This flow field will hereby be called flow field 1.

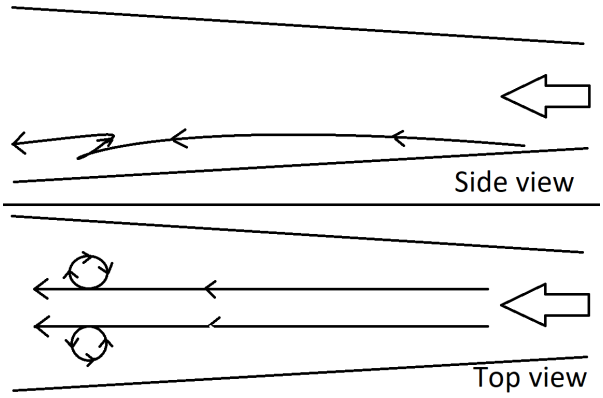

Figure 18: Flow field 1. Stable flow field from the exit of venturi with wet gas flow.

The second flow field that can be generated from the backward flow as shown in Figure 19 occurs when the liquid starts to accumulate in the in the swirl. This results in a buildup of liquids in the divergent part of the venturi. The buildup increases in height until the wet gas flow separates off a layer from the accumulated liquid as depicted in figure 20. This process repeats with different magnitudes apparently at random time intervals ranging from some centiseconds to a second. This flow field generates a substantial higher magnitude of pulsations in the flow than the first flow field. It can also be noted that the mass flow fluctuates with the separations of the liquid layers, and that the flow regime after the venturi is highly dispersed. This flow field will hereby be called flow field 2. A thorough description of venturi swirls is done by Mehlum [17].

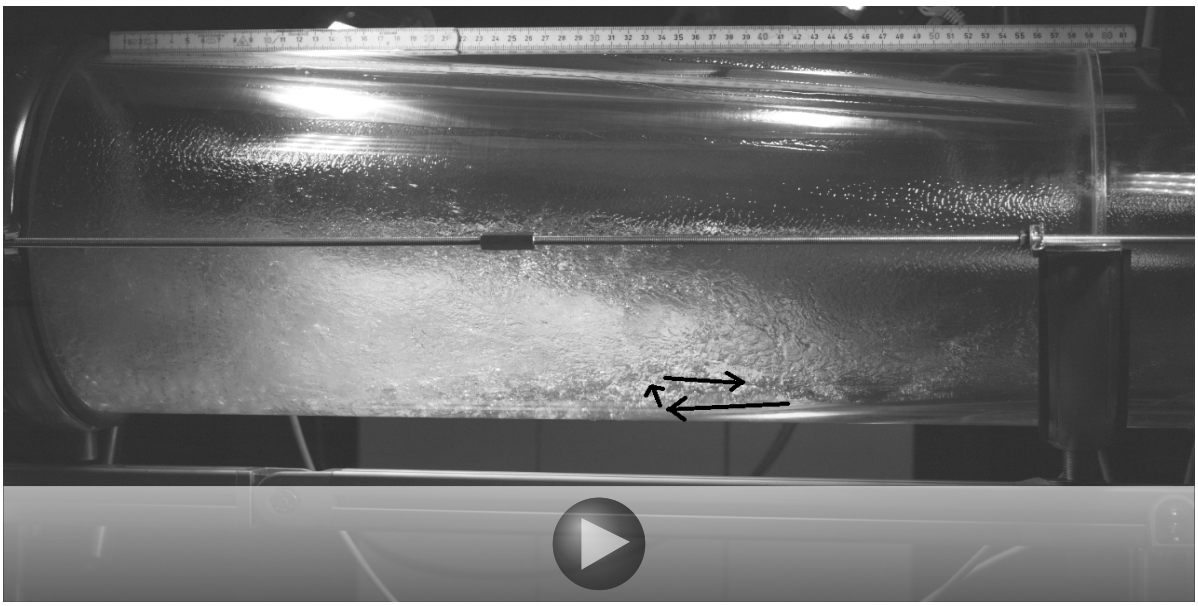

Figure 19: Flow field 2. Venturi exit with a GMF of 0.90 -and stratified flow at the entrance. This is also a video played at normal speed. (If not able to view it, see Appendix E for guide)

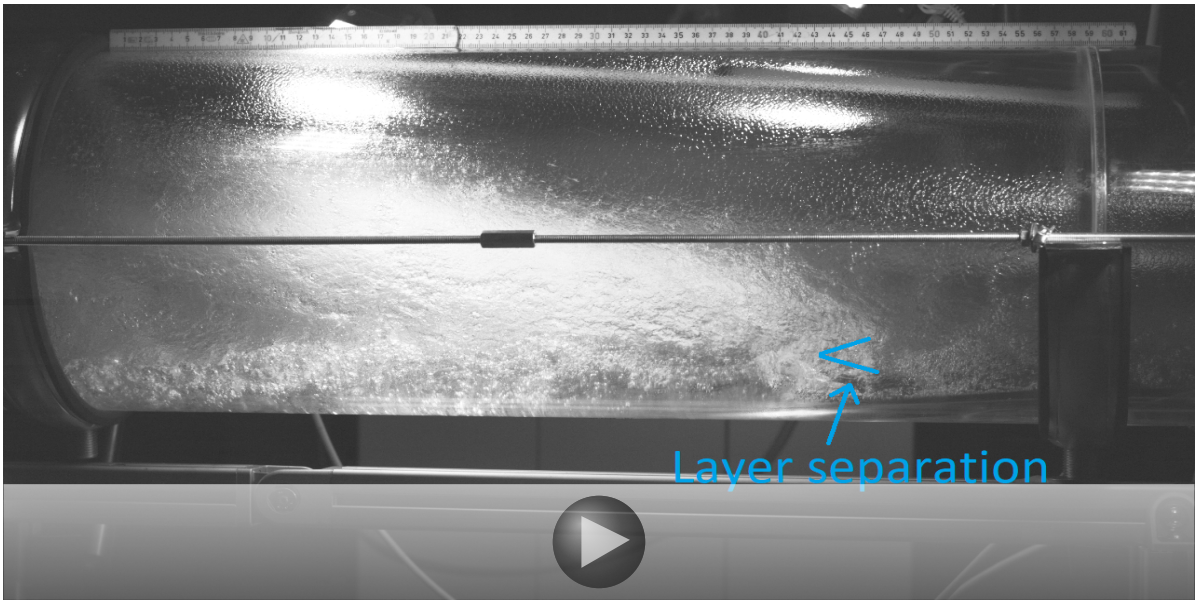

Figure 20: Venturi exit with a GMF of 0.90 -and stratified flow at entrance. This is also a slow motion video with play speed 100 times slower than real time. (If not able to view it, see Appendix E for guide)

6.3.2 Torque

The torque measurements show the largest impact from the flow fields generated by the venturi. Figure 21 shows the difference in TQ measurement for GMF 0.90 without venturi, dispersed flow and stratified flow. The figure shows a significant increase in the spread of the data when adding the venturi to the system. It is also a considerable

difference from the dispersed to the stratified case, where the dispersed case has a smaller deviation range and no major spikes in the data. For the stratified case, there are multiple spikes in TQ and the data do not center around the average. For numerical comparison of the graphs, the standard deviation[1] was found most suitable.

For the dispersed case, the venturi produced flow field 1, with no accumulation of liquids. The pulsations generated from this flow makes the torque pulsate around the average with a standard deviation 5 times higher than the without venturi.

The stratified flow produced flow field 2, where liquid accumulates in divergent part of the venturi and periodically the gas separates off a layer of liquid. When the liquid is building up in the venturi the GMF in the flow is increased and when the gas separates off a layer of liquid the GMF is decreased for a short interval. This means that the spikes appearing in the chart represent a periodic lower GMF and, further, that during the buildup of liquid the torque is lower than the reference without the venturi. This dynamic variation in GMF can potentially cause higher wear on the compressor components and have negative effects on control systems for the compressor.

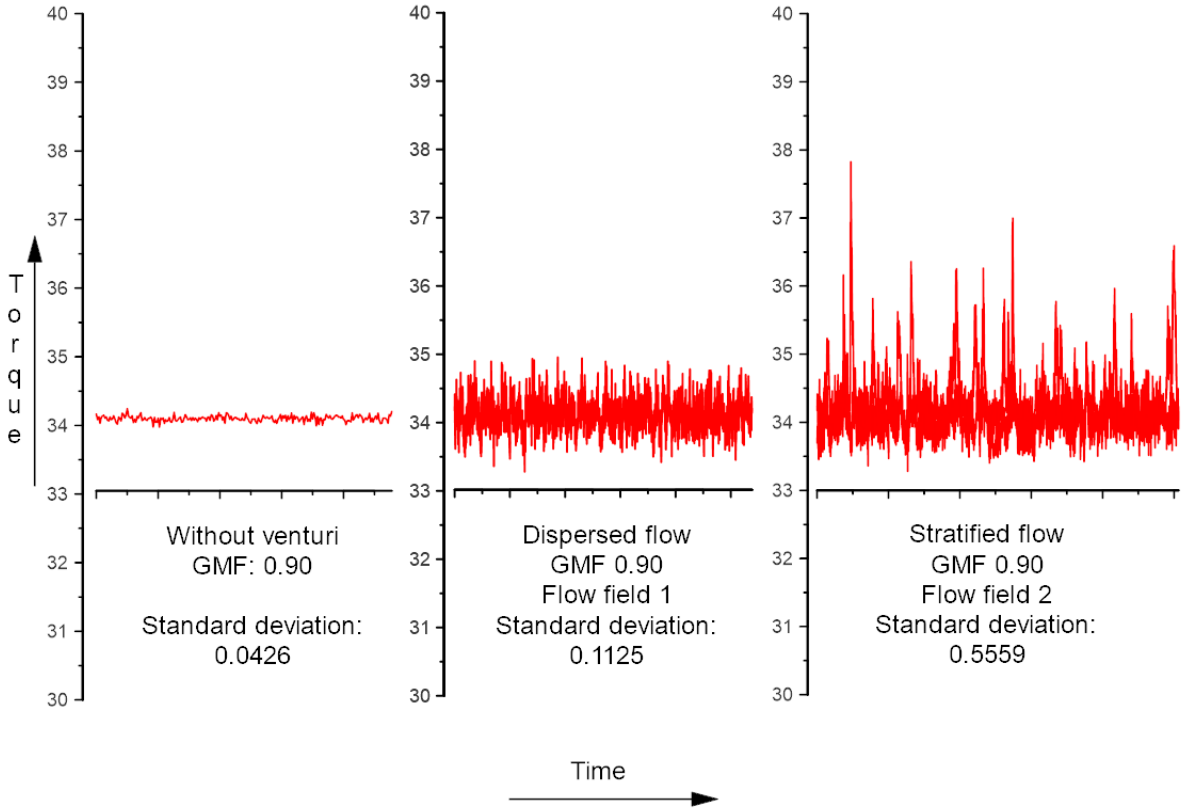

Figure 21: Torque measurements with GMF 0.90 for dispersed flow, stratified flow and without venturi

[1]In some instances, a slight variation of standard deviation was used to account for the average decline or increase during the whole period. This variation was to divide the data into smaller sets to minimize the impact on the results.

The spikes in TQ increase the standard deviation to 13 times higher than for the case without the venturi. Figure 22 shows how the standard deviation of TQ changes with GMF for the baseline without venturi, dispersed and stratified flow. The dashed line marks where the flow field changes to flow field 2. The figure shows a gradually increase in the standard deviation with decreasing GMF. The case without venturi has the lowest standard deviation, followed by the dispersed case and lastly stratified has the highest standard deviation. The differences between the cases diverge with decreased GMF. The dispersed case shows a significant jump in standard deviation after change in the flow field. A stratified flow regime is more asymmetrical than a dispersed flow regime and generates unstable flows at higher GMF. It seems to be associated with higher standard deviations of the results at higher grade of stratified flow.

From general observations during testing of the venturi, a higher grade of dispersed flow than for the defined cases did not generate flow field 2 for any GMFs. Based on these observations and the collected data a general increase in the standard deviation for the torque with higher degree of stratified flow is shown.

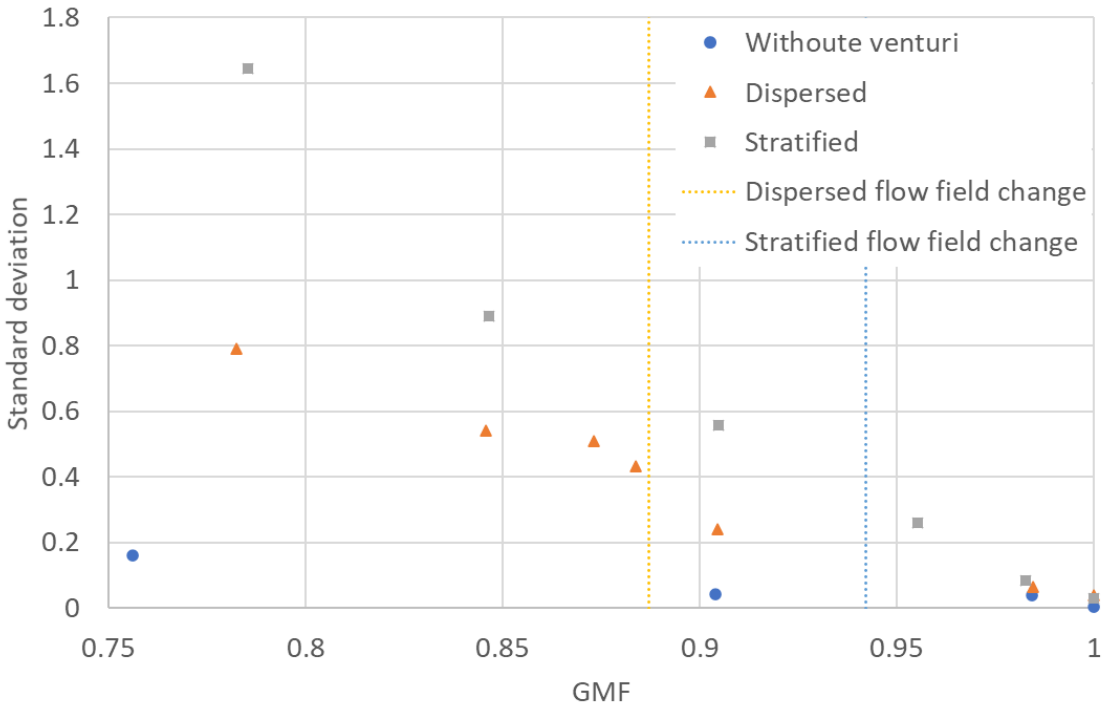

Figure 22: The standard deviation of torque measurements.

Figure 23 shows the torque accompanied with the rotational speed for stratified flow at GMF 0.78. During this flow conditions the venturi generates flow field 2 where liquids builds up and periodically reenter the stream in sudden bursts. The figure shows that the spikes in torque follow a drop in the rotational speed. The spikes in TQ overcorrect the drop in rotational speed likely due to the monetary spike in GMF has ceased faster than the control system can react.

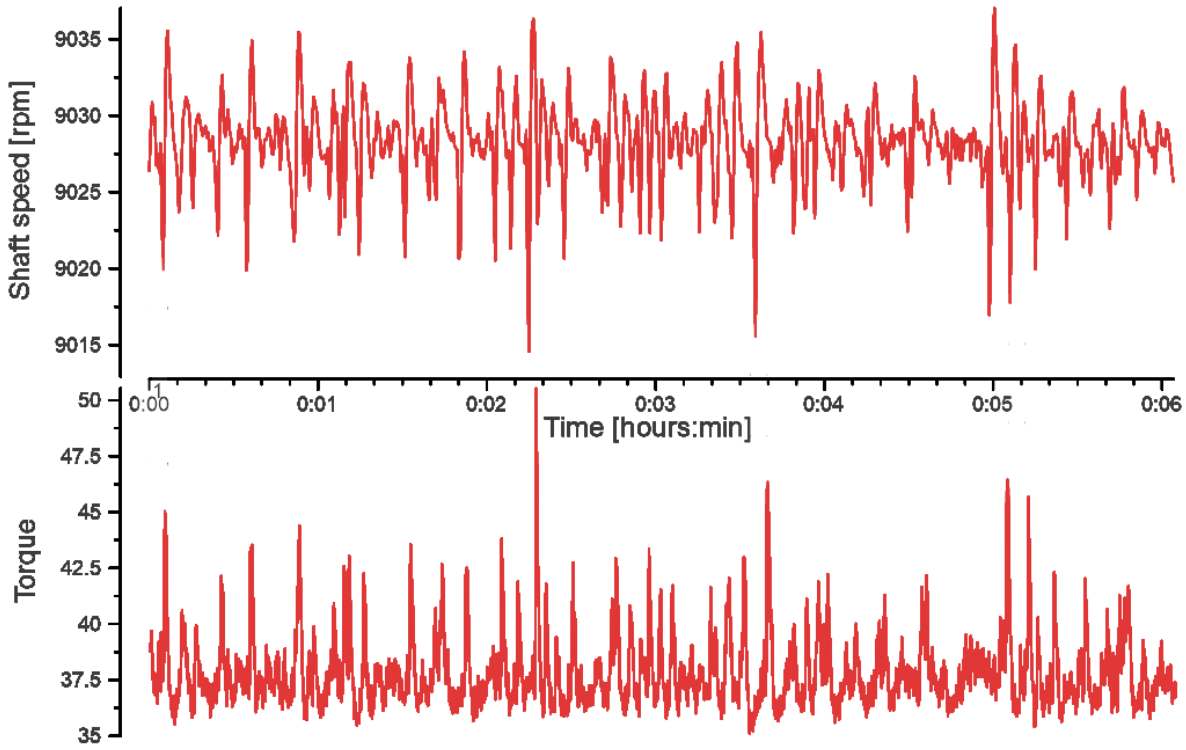

Figure 23: Torque and the rotational speed of the impeller for stratified flow and a GMF of 0.78.

Figure 24 shows the torque for dispersed flow with GMF 1/0.98/0.90/0.85/0.78. The figure shows that TQ increases and becomes more volatile with decreasing GMF. Since TQ -and the standard deviation of TQ measurements have a directional connection to the GMF and the flow regime, then TQ and the standard deviation of TQ should be sufficient to define mathematical correlations between these parameters based on experimental data. However, it is currently not sufficient data to extrapolate these correlations. Implementation of this parameter will be further discussed in chapter 7

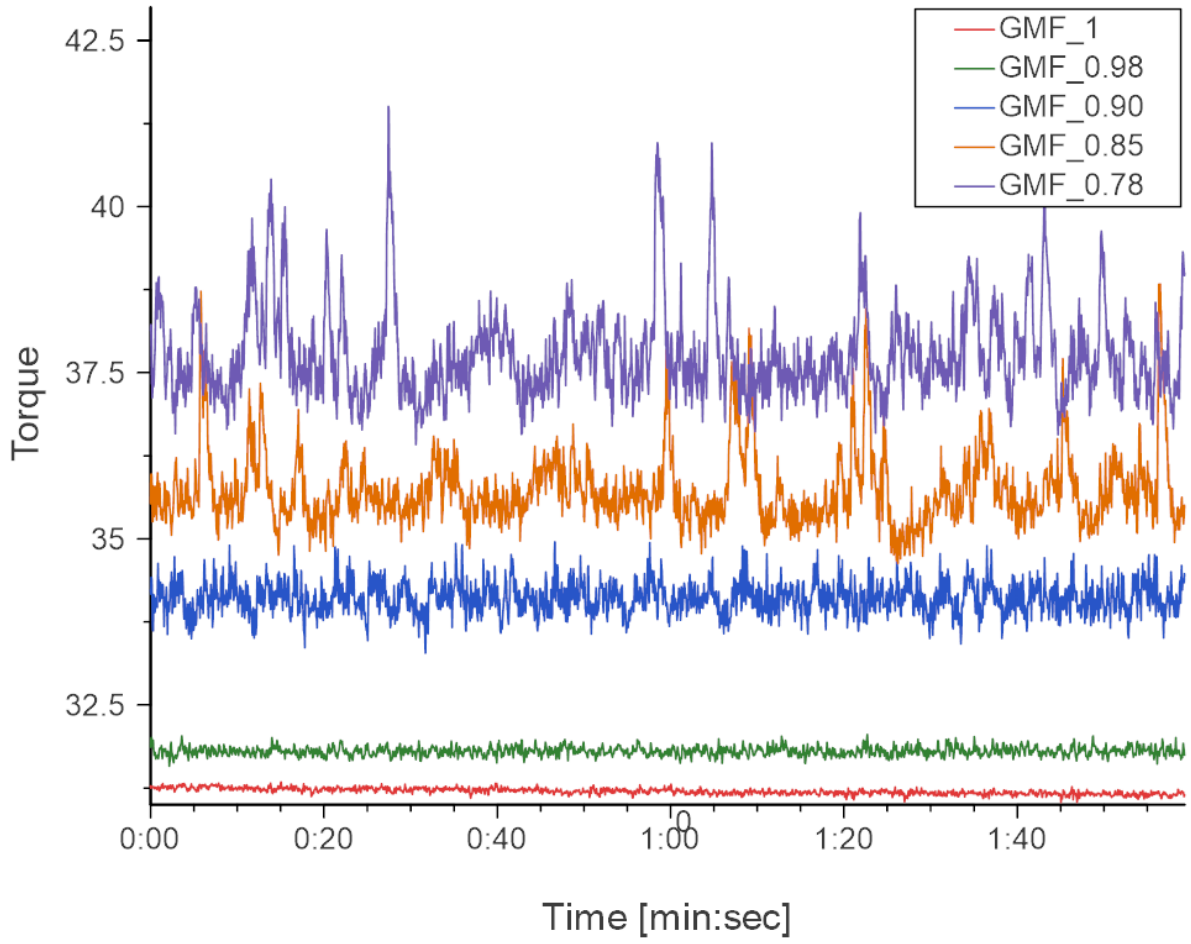

Figure 24: Torque measurements for dispersed flow.

6.3.3 Inlet pressure

The compressors inlet pressure P_1 shows some similar tendency as the torque. Figure 25 shows P_1 for GMF 0.90 without venturi, dispersed flow and stratified flow. The fluctuations for the test without venturi and the test with dispersed flow are similar, while the stratified case has substantial larger fluctuations with a standard deviation 5 times higher. It should be noted that there are no major spikes in the measurements as were observed for the torque measurements.

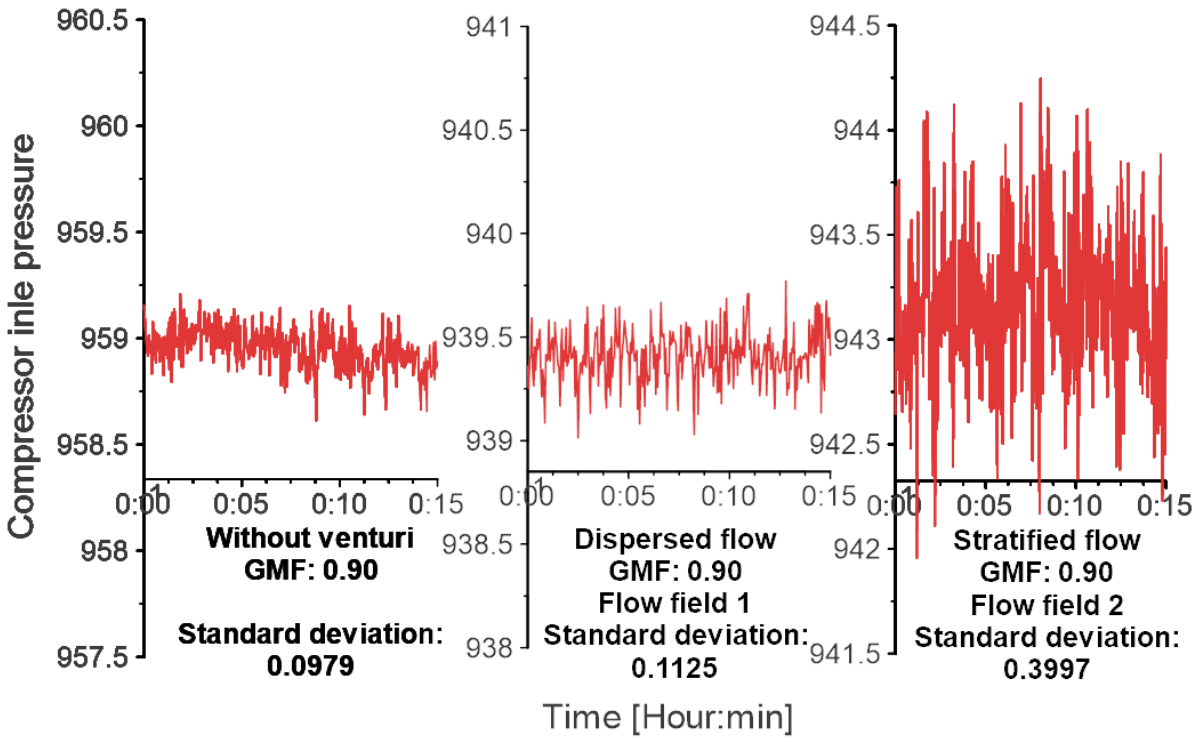

Figure 25: Compressor inlet pressure measurements with GMF 0.90 for dispersed flow, stratified flow and without venturi.

Figure 26 shows the standard deviation for the P_1 measurements against the GMF for the case without venturi, dispersed case and stratified case. The stratified case has the highest standard deviations in P_1 measurements for both flow field 1 and 2. While there is no significant difference between dispersed with flow field 1 and without venturi. When the dispersed case starts to generate flow field 2 there is a decisive jump to about twice as high standard deviation than without venturi. It seems like the pressure is more dependent on the inlet flow regime than the torque is.

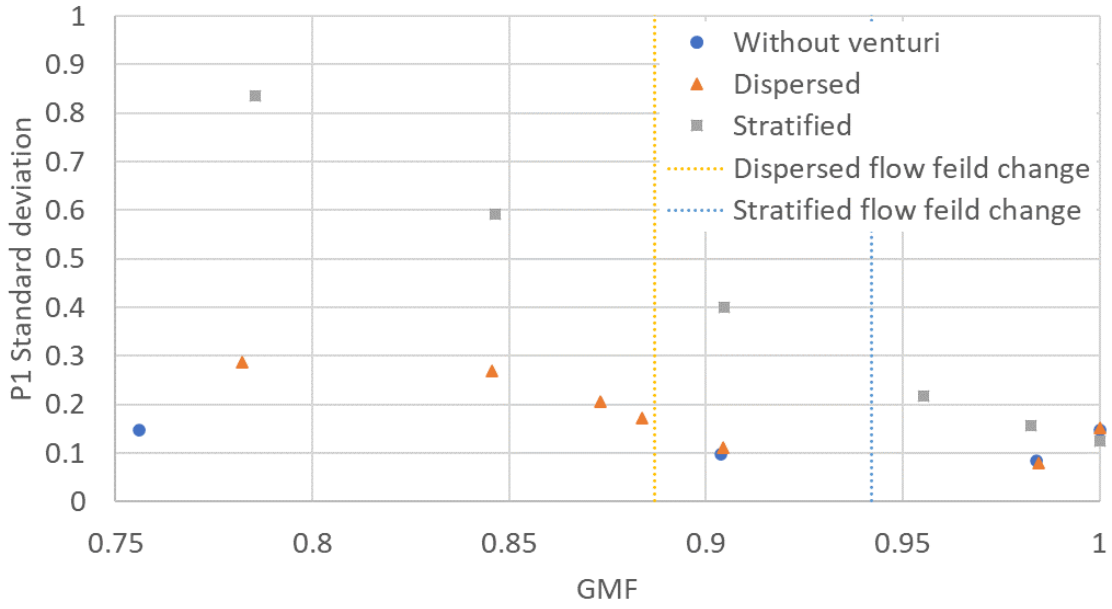

Figure 26: The standard deviation of P_1 measurements.

6.3.4 Measurement accuracy of the venturi

To validate the accuracy of the venturi, the mass flow of the orifice and the venturi are compared. For dry conditions there are well established ISO standards for both orifice and venturi ISO:5167 [9]. While there is an ISO standard that corrects for wet gas conditions ISO/TR:11583 [2], the range of parameters for this standard is limited. Some of the limits with regard to the venturi, are that the density ratio (δ) of the wet gas should be higher than 0.02, $Fr/\beta^{2.5}$ should be higher than 3 and the Lockhart-Martinelli parameter (X) should be lower than 0.3.

A wet gas consisting of air and water have a density ratio of 0.00125 at atmospheric conditions. For the flow conditions during the cases evaluated in the present study $Fr/\beta^{2.5}$ reached up to 1.73 and the Lockhart-Martinelli parameter was between 0 and 0.019. It can be noted that the Lockhart-Martinelli parameter for the majority of the tests are below 0.016 witch is associated with a larger uncertainty in the wet gas correction and from uncertainty calculations from ISO/TR:11583 the uncertainty is at highest 3.04%.

Even if the cases are outside the range of the standard ISO/TR:11583, it is decided to utilize the standard's correction factor to correct for over-estimating mass flow in the venturi during wet gas conditions. It can be noted that the orifice will, during all cases, operate in dry conditions.

Figure 27 shows the ratio between calculated mass flow between the orifice and the venturi, with and without wet gas correction. Both the dispersed and stratified case without correction over-predict mass flow through the venturi with an increasing degree at decreasing GMF. The dispersed case has a slightly higher over-estimation of the mass flow. When utilizing wet gas correction the mass flow is underestimated and diverging from the orifice mass flow estimation with decreasing GMF.

Even when accounting for uncertainty of the orifice the mass flow calculations are outside the uncertainty given in ISO/TR:11583. This is to be expected when using the standard well outside its range. When accounting for the venturis slightly higher mass flow estimation at dry conditions it seems like the wet gas correction over-corrects the mass flow by about the double, resulting in no more accurate mass flow estimations than when not utilizing wet gas corrections.

The calculations are performed in programming language Python and uses the thermophysical property library of CoolProp [18]. The code of the calculations is given in Appendix D.

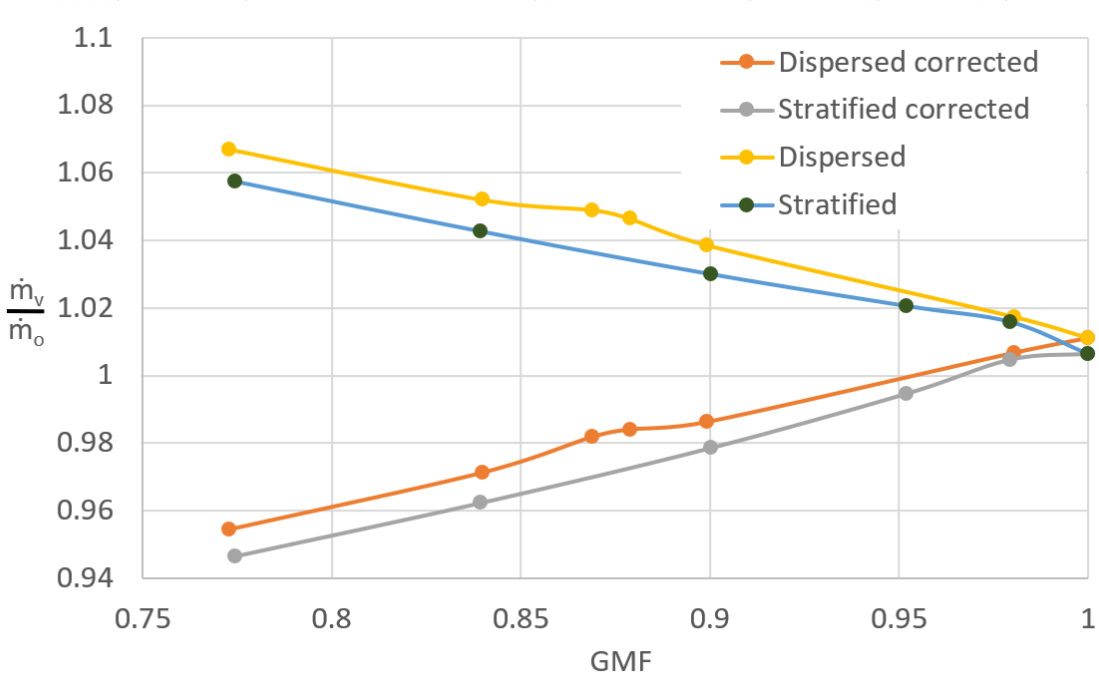

Figure 27: Difference in calculated mass flow between the orifice and the venturi.

6.3.5 Pressure loss in venturi

Inside the venturi the flow velocity is substantially increased and thus is more inclined to pressure loss from friction. Additionally, the flow fields generated are expected to generate some pressure loss. Figure 28 shows the measured pressure loss over the venturi. At GMF 1 the cases should be identical so the pressure loss should also be the same. The figure shows a slight difference at GMF 1 with 0.4 millibar considering that this measurement utilizes P_1 with 900+ millibar this can be considered acceptable measurement error for the sensor. The stratified case shows slightly higher pressure loss over the venturi than the dispersed case. It is also a distinct jump in pressure loss associated with flow field 2, which is expected due to the more turbulent nature of flow field 2.

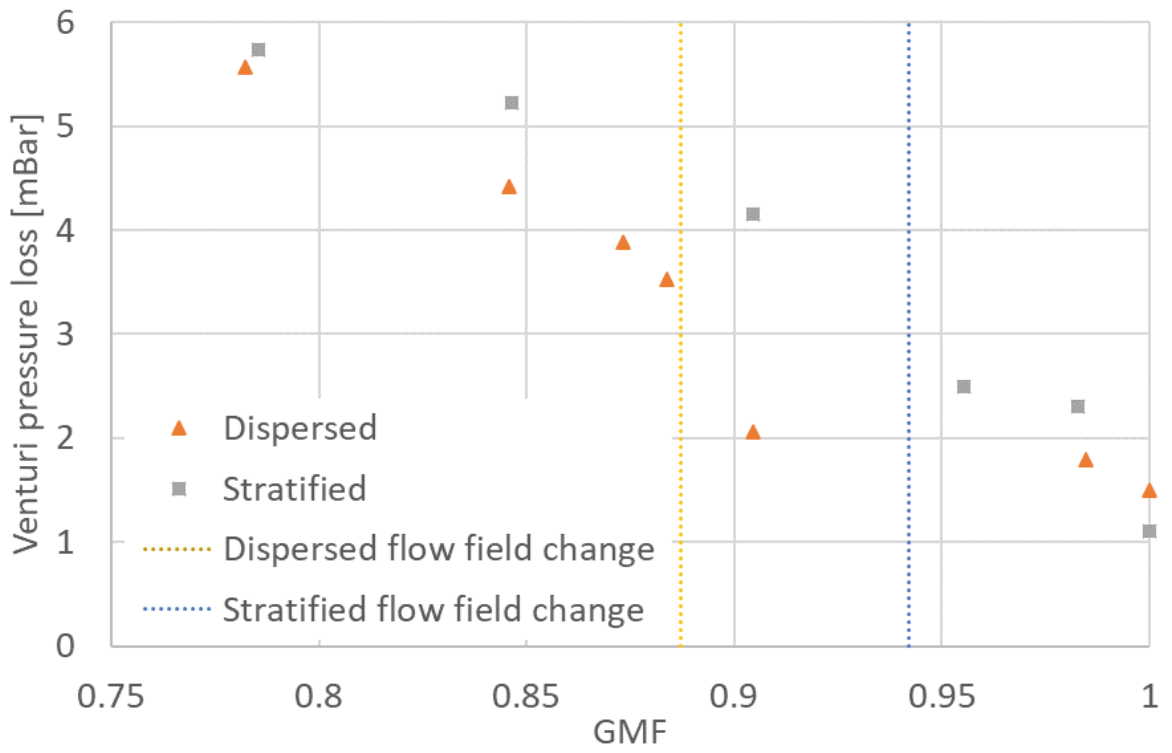

Figure 28: Measured pressure loss over the venturi.

6.3.6 Polytropic efficiency

The normalized polytropic efficiency (η_P) for the cases are plotted against GMF in figure 29. To consider the pressure loss caused by the venturi, separate calculations of η_P have been done with the pressure loss added to P_1 to illustrate the efficiency impact of the system. All cases show a decrease in η_P with decreasing GMF. This is due to various wet gas effects e.g changes in compressibility -and Mach number, generation of liquid films on the compressor components and slip between phases. The wet gas effects are well documented by Hundseid et al. [19].

The case without venturi has the highest efficiency at high GMF and falls to the lowest efficiency at low GMF. Notice that the lowest GMF measurement point is significantly lower than the cases for the venturi, this makes the comparison between the cases less reliable.

The stratified flow has higher efficiency than the dispersed flow for high GMF. After the dispersed flow changes to flow field 2, with liquid buildups, then the dispersed case bypass η_P of both the stratified case and the baseline without the venturi. When accounting for the pressure loss the same tendency is observed with a slight downward offset that increases with decreasing GMF.

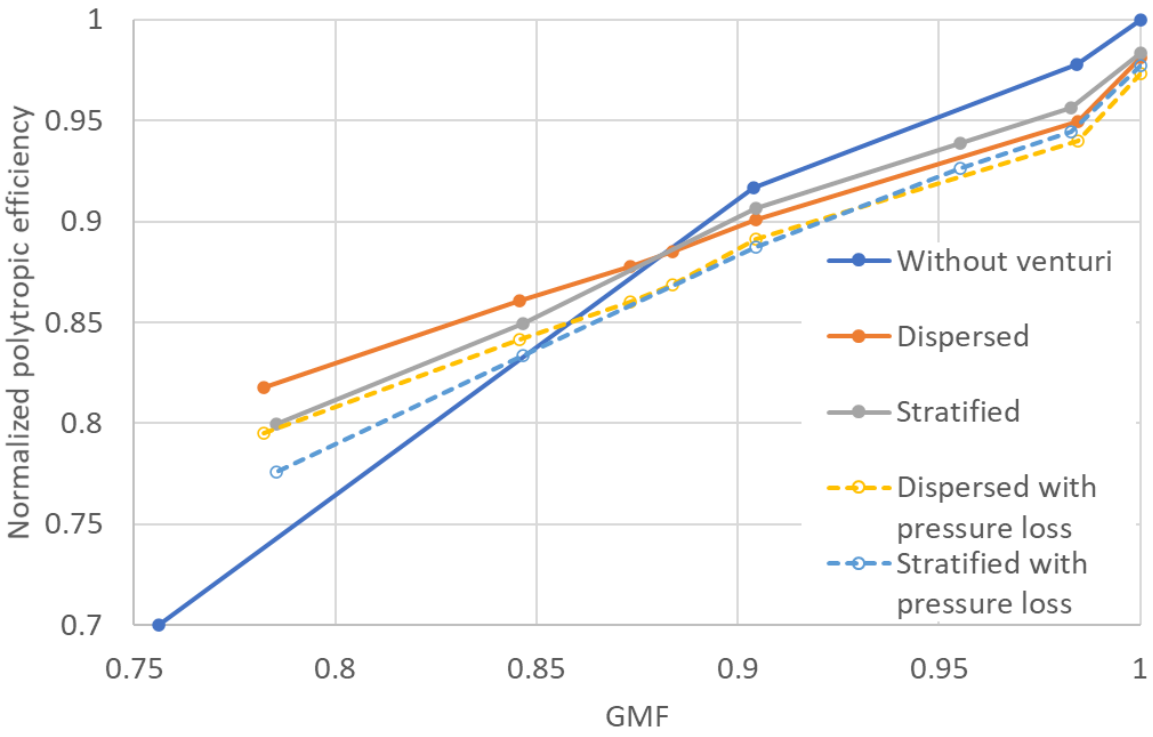

Figure 29: Normalized polytropic efficiency against GMF.

This figure indicates that the flow field generated from the venturi has a beneficial influence on η_P. This beneficial influence seems to be connected to the dynamic flow field 2 described in 6.3.1. This result is quite unexpected. The expected result would be that the venturi when not accounting for the pressure loss, would have no or a slight negative effect at GMF 1 and that the negative effect would increase with decrees in GMF. Further, a distinct fall in η_P would be expected as a result of the change to flow field 2 due to the flow no longer being stable.

One theory explaining the increase in efficiency is that the unstable flow generated from flow field 2 causes the flow regime after the venturi to be highly dispersed. Due to the close proximity between the venturi -and compressor, the flow field entering the compressor is also highly dispersed. With a more dispersed flow regime, the liquid phase will be more inclined to behave as the gas flow and thus reducing the two-phase effects in the compressor. This theory is supported by work done by Fabbrizzi et al. that concludes that smaller droplet size in wet gas grants substantially better compressor performance [20]. This theory suggest that the venturi could be used for both flow measurements and wet gas atomizing.

The venturi causes a slight decrease in the mass flow that have some impact on η_P that is not reflected in the figure. However, this low difference at about 3% cannot account for unexpected findings in the data.

6.3.7 Frequency analysis

An FFT analysis is performed on dynamic pressure sensors in the diffuser and before -and after the venturi. Figure 30 and 31 shows a 3D representation of the amplitude of pressure versus the frequency over a time interval for the pressure before -and after the venturi respectively. Both display the same trend while the amplitude of the pressure peaks before the venturi are lower than after the venturi. A logarithmic amplitude scale is used to be able to see the low amplitudes spikes in comparison to the severe spikes at low frequency. At low frequency 1-10 Hz amplitude spikes are 2 to 3 orders of magnitude higher than the remaining amplitude spikes and seem to be noise generated from general changes in the flow. The next major amplitude spike is at 2695 Hz and all subsequent spikes are at intervals of 2695 Hz. This frequency corresponds to the blade pass frequency of the compressor. No other notable frequency was found for any of the cases. This appears to indicate that the pulsations generated by the venturi are occurring at random intervals.

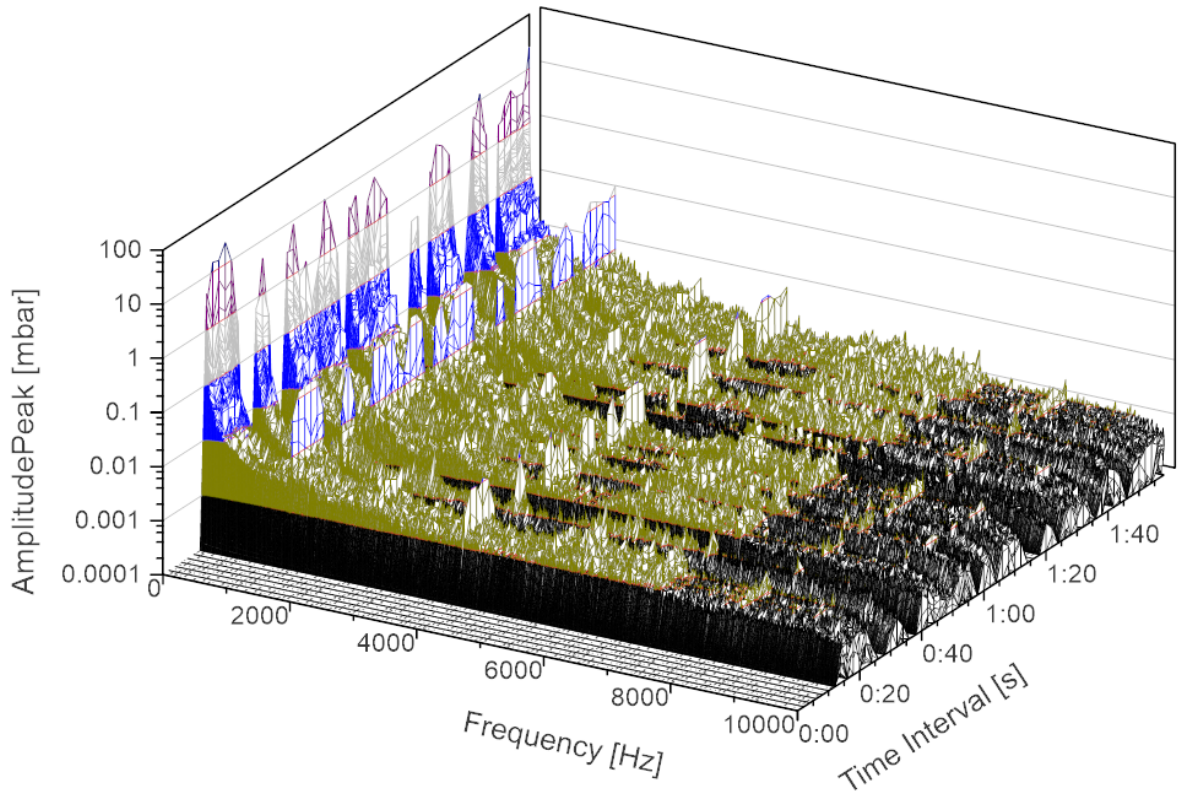

Figure 30: FFT analysis of pressure before the venturi for dispersed flow with GMF 0.90.

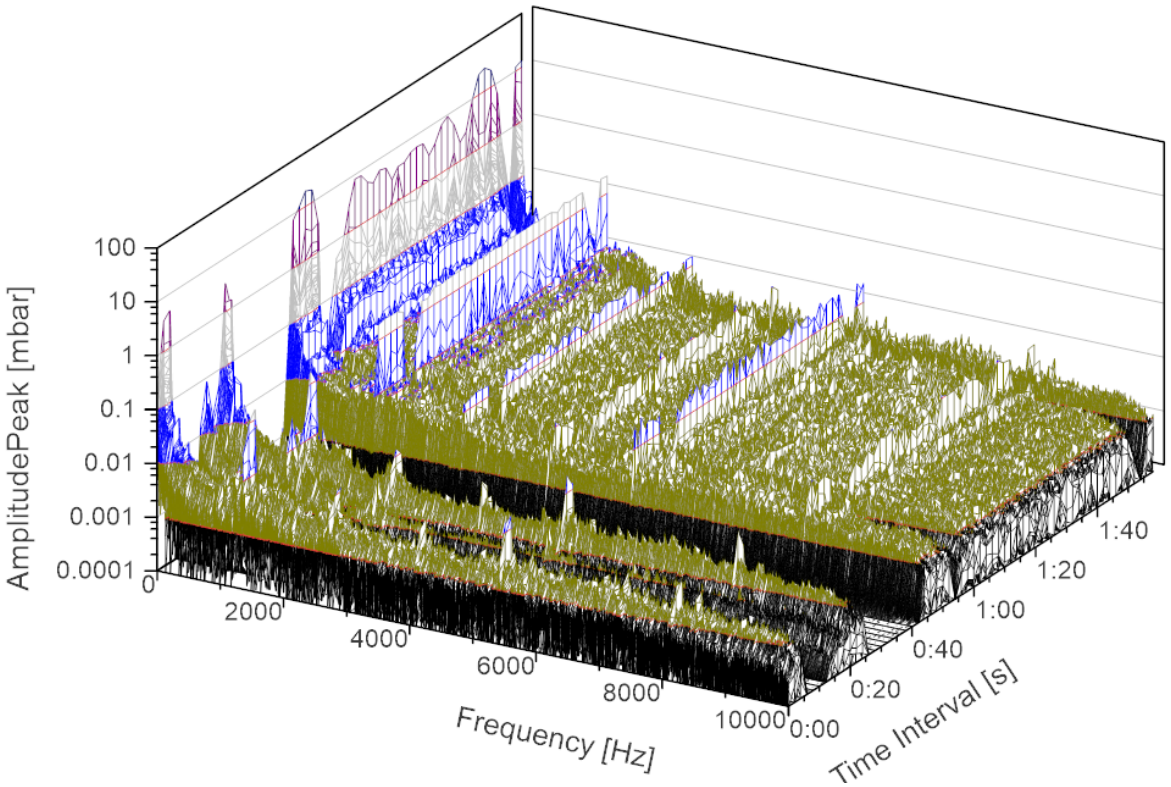

Figure 31: FFT analysis of pressure after the venturi for dispersed flow with GMF 0.90.

Figure 32 shows a 3D representation of the amplitude of dynamic pressure at the z-axis the frequency at the x-axis and time interval at the y-axis for the flow in the diffuser at GMF 0.90 with dispersed flow before the venturi. While Figure 33 shows a 3D representation of the amplitude of dynamic pressure at the z-axis the frequency at the x-axis and time interval at the y-axis for the flow in the diffuser at GMF 0.90 with stratified flow before the venturi.

The figures show that there is a major spike at 1Hz and then major spikes at intervals of 2695 Hz, the corresponding to blade pass frequency. The depressed flow generates a stable flow in the venturi and stratified flow generates an unstable flow. The stratified FFT shows lower amplitude in the pressure then the dispersed FFT.

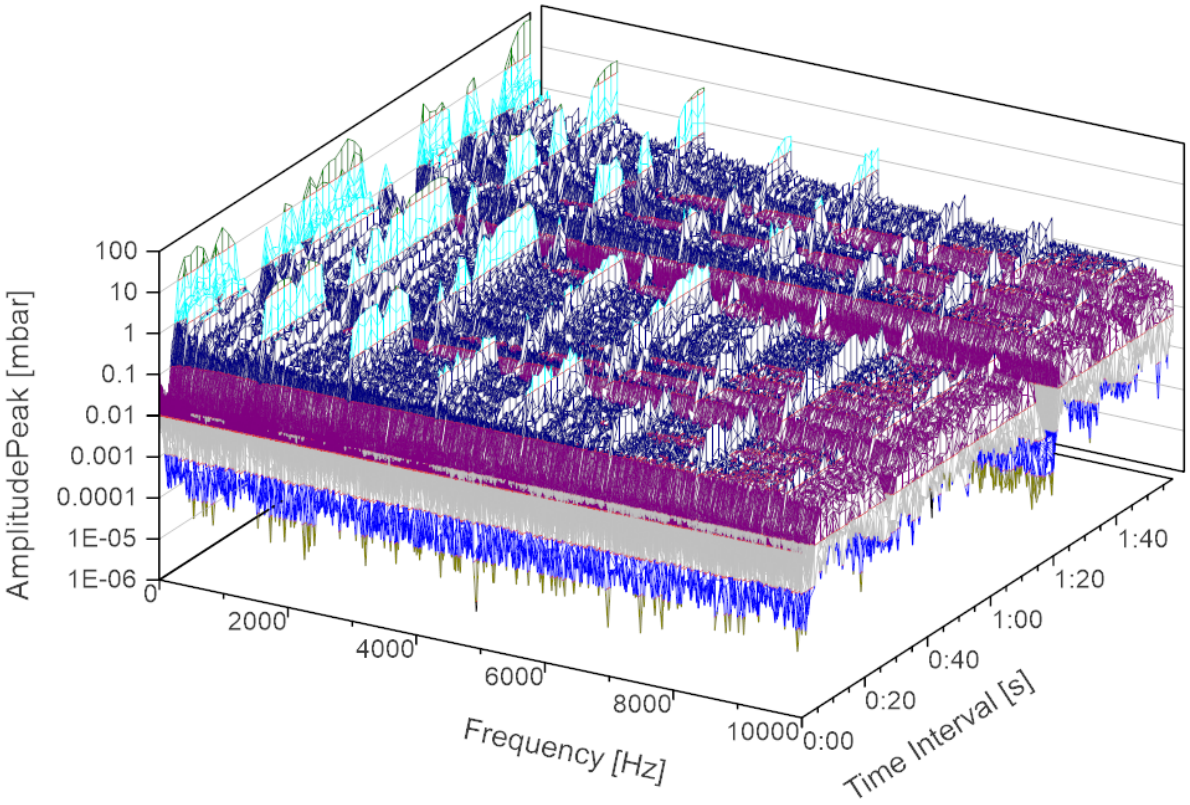

Figure 32: FFT analysis of pressure in the diffuser for dispersed flow with GMF 0.90.

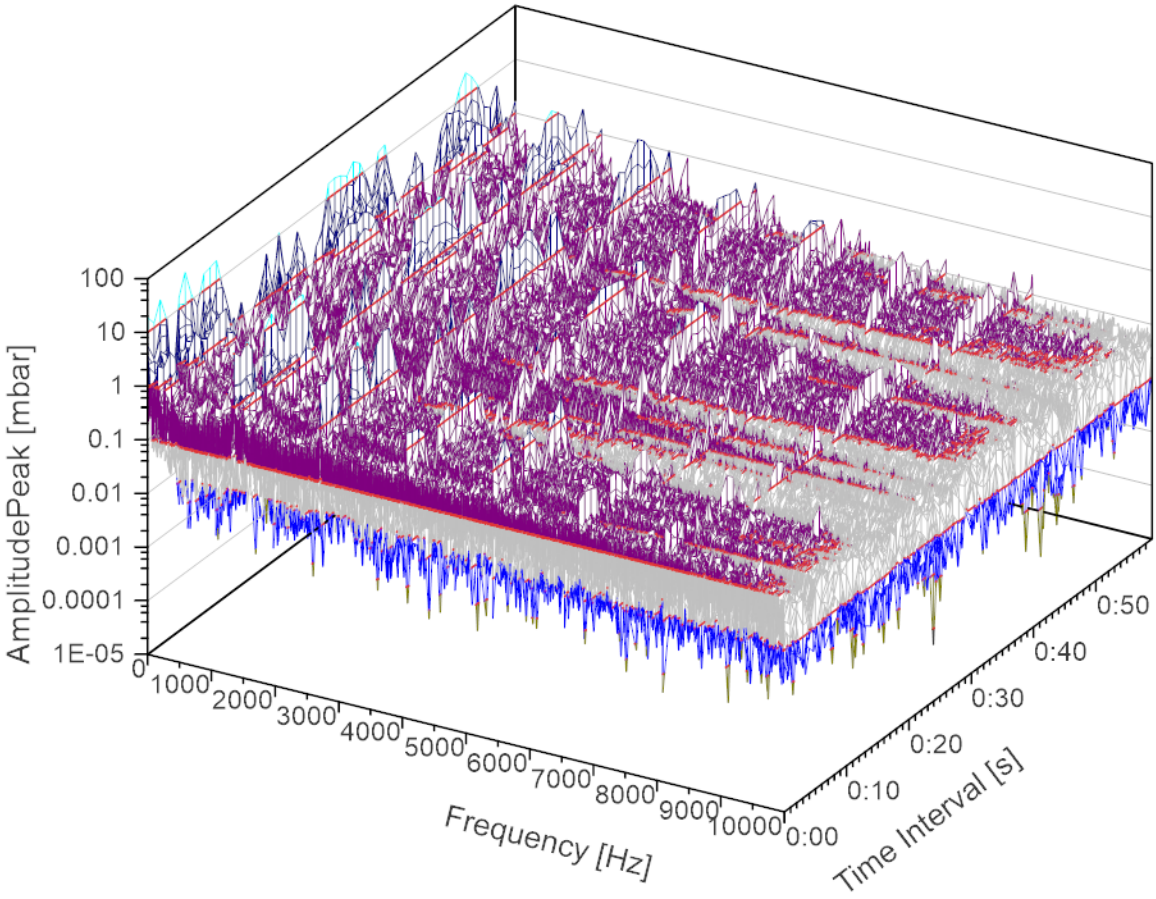

Figure 33: FFT analysis of pressure in the diffuser for stratified flow with GMF 0.90.

6.4 Summary

In this chapter the results from the experimental camping have been presented and discussed. The most prominent results appear to be that the torque measurements magnitude and volatility should be able to correlate to the GMF and flow regime based on empirical data. Further, that the venturi causes liquid swirls that can dynamically change the GMF that enters the compressor and that, in general, the venturi causes more volatility in measurements in the compressor system. Finally, it is indicates that the venturi can be beneficial to the η_P of the compressor.

7 Digital model

This chapter will focus on functionality, parameters of interest and challenges regarding a digital model for control and optimization a compressor system for wet gas flow utilizing a horizontal venturi for flow measurements.

7.1 The digital model

The data analyzed showed considerable promise for the torque measurement to be used for determine the GMF and flow regime. Further, the GMF and flow regime can be utilized to improve the accuracy of the flow measurements by the venturi. The magnitude of the torque shows direct proportionality to the amount of liquids in the wet gas as shown in figure 34 and the volatility in the torque measurements shows proportionality with the GMF -and flow regime. To consider the slight decrease in mass flow caused by the decreasing GMF in the case data, the torque is divided by the mass flow of gas for a better representation of the almost linear relation. The figure shows that the stratified case requires a slightly higher torque than for the dispersed case, for a given GMF.

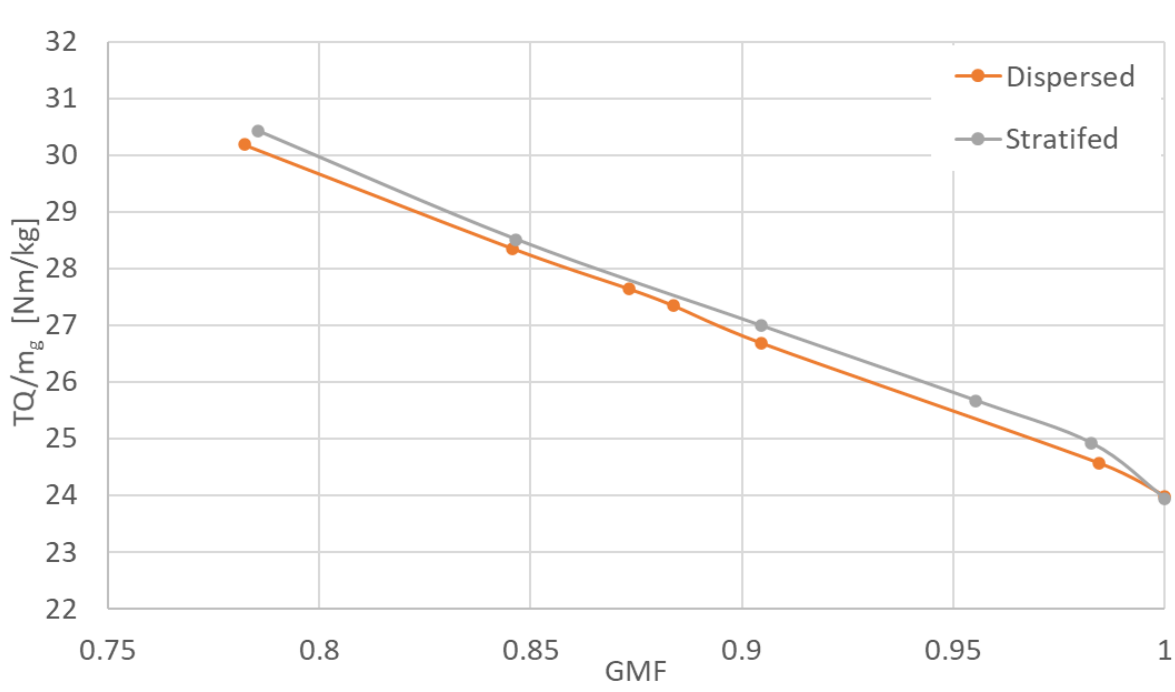

Figure 34: Torque divided by mass flow against GMF

In order to find the flow regime, flow-regime-maps or the standard deviation of the torque may be used. Figure 35 shows the standard deviation of TQ against GMF and is discussed in detail in 6.3.2. The figure shows that the standard deviation and the GMF can be used to find the flow regime. Now GMF can be found with the flow regime and

vice versa. With an iterative process with appropriate start estimates for GMF -and the flow regime, the system can be solved. The first part of the iteration should find GMF, this is due to flow regime having a smaller impact on the result. By using the GMF and flow regime from the previous measurement point calculations in the next calculation removes the need to iterate the calculations.

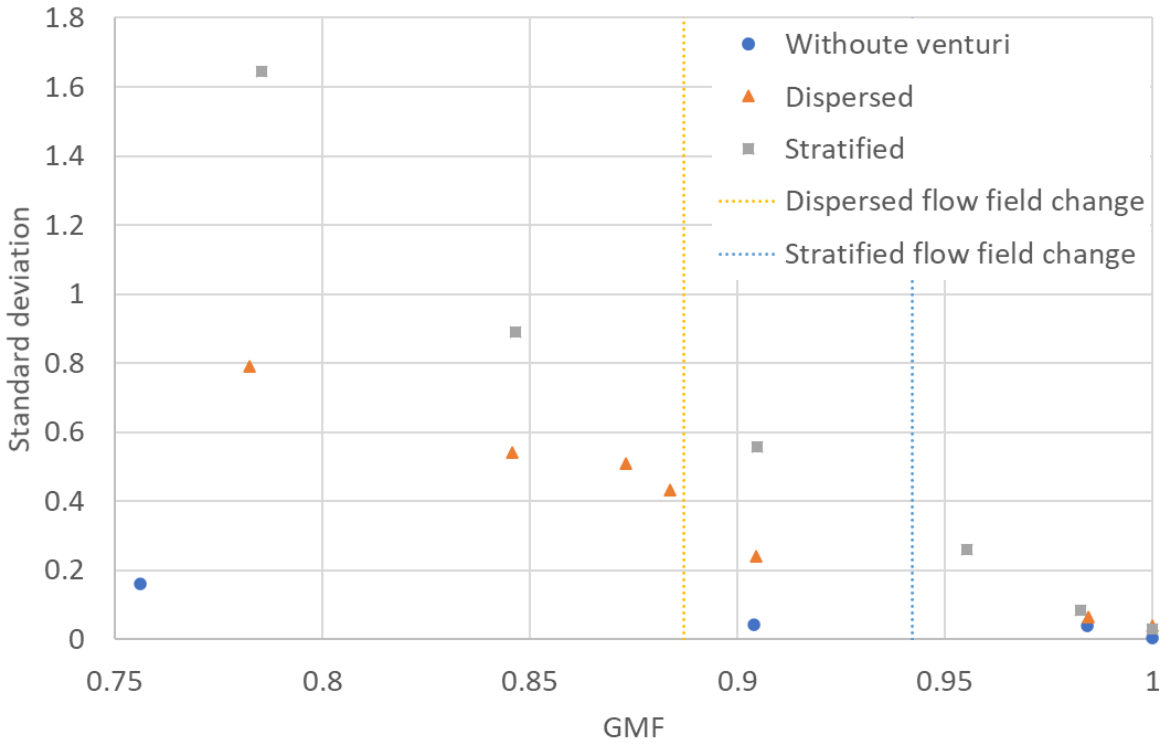

Figure 35: The standard deviation of torque measurements.

To use the torque measurements, in order to find flow parameters, an average torque should be used after the volatility reaches a certain point of fluctuations. The average should not be done over a long period to minimize the effect from increasing or decreasing trends in the data that will inherently offset the average to half the period. On the other hand, the average should not be too short to avoid that the average contains large spikes. To mitigate the offset of the average a weighted average can be used where the latest measurements has a higher weight. Further, to mitigate the effect of large spikes each value can be square rooted while the sum is squared. Equation 7.1 shows a possible weighted average where x_i is the latest measurement, the numerical values of the weights and the exponent of the measurements can be change to suitable numbers.

$$Weighted\ Average = \left(\frac{\sqrt{x_1} + 2\sqrt{x_2} + 3\sqrt{x_3} + \cdots + i\sqrt{x_i}}{1 + 2 + 3 + \cdots + i} \right)^2 \tag{7.1}$$

7.2 Building the data set

When making characteristics of the for TQ, SD, flow regimes, mass flow an GMF, the test matrix should be mass flow and GMF as the test parameters, measure TQ and SD for each combination as shown in matrix 7.2. Then this test Matrix should be applied for several flow regimes. Moreover, if it is to be used by a variable drive compressor, the same procedure should be applied for several rotational speeds ending up with a 4-dimensional test matrix shown in Matrix 7.3.

$$A = \begin{array}{c|cccc} & GMF_1 & GMF_2 & \dots & GMF_j \\ \hline \dot{m}_1 & TQ_{11}, SD_{11} & TQ_{12}, SD_{12} & \dots & TQ_{1j}, SD_{1j} \\ \dot{m}_2 & TQ_{21}, SD_{21} & TQ_{22}, SD_{22} & \dots & TQ_{2j}, SD_{2j} \\ \vdots & \vdots & \vdots & \ddots & \vdots \\ \dot{m}_i & TQ_{i1}, SD_{i1} & TQ_{i2}, SD_{i2} & \dots & TQ_{ij}, SD_{ij} \end{array} \tag{7.2}$$

$$Test\ matrix = \begin{array}{c|cccc} & \Omega_1 & \Omega_2 & \dots & \Omega_j \\ \hline FR_1 & A_{11} & A_{12} & \dots & A_{1j} \\ FR_2 & A_{21} & A_{_{22}} & \dots & A_{2j} \\ \vdots & \vdots & \vdots & \ddots & \vdots \\ FR_i & A_{i1} & A_{i2} & \dots & A_{ij} \end{array} \tag{7.3}$$

7.3 Challenges regarding the model

Firstly, the data gathered are only for wet gas flow with air and water. Studies done by Reader-Harris et al. [21] and Britton et al. [22], shows that altering liquid properties changes the response of the system regarding the over-reading mass flow. Even though these findings are specific to over-reading, parallels can be drawn to the remaining wet gas interactions in the venturi. Thus, care is advised in regard to draw direct parallels to other wet gas combinations without further investigations of wet gas interactions in venturis.

Secondly, due to the model's dependence on averages the model will not be able to promptly react to fast changing parameters. This can be a critical issue concerning compressor surge and other safety features. Therefore, this model should only be used as a supplement to other control systems, and particular care is advised when using the model in combination with other control systems that requires fast response.

Thirdly, the flow regime found is the regime before the venturi. Due to the venturi ability to periodical altering the flow regime, the flow regime found will not always be the same regime as entering the compressor.

8 Conclusion

Several noticeable interactions between the venturi and the compressor were detected in the present work and a potential digital model to determine GMF and flow regime was proposed. Two main types of flow fields in the divergent part of the venturi were found. Firstly, flow field 1, a stable flow with some backward flow, caused a larger volatility of the inlet pressure and torque for the compressor. Secondly, flow field 2, an unstable flow where liquid accumulates in the divergence part of the venturi with periodically large proportion of the accumulated liquids reentering the wet gas flow. This flow field caused a larger volatility along with periodically severe spikes in inlet pressure and torque. With this particular flow field there will be a constant change in GMF, which can cause severe problems with control systems and increasing the wear on the system resulting in a decreased reliability.

An unexpected increase of polytropic efficiency caused by the venturi at low GMF was documented. One theory to explain this is that the unstable flow of flow field 2 causes the flow regime after the venturi to be highly dispersed, which can result in less wet gas interactions in the compressor. These results are based on a limited amount of data and should therefore be investigated further before application.

The proposed digital model utilizes the magnitude and the volatility of the torque measurement to find the GMF and flow field. This can further be used to better predict the mass flow from the venturi.

Overall, the increase in η_P seems promising but the unstable flow generated by the venturi has potentially severe negative effects on the reliability of the compressor system. Therefore, further extensive research should be done before utilizing horizontal venturi, especially with low GMF wet gas flow and/or for systems that depend on high reliability.

8.1 Future Work

To investigate further the effects the venturi have on compressor systems, especially η_P will be important. This can have the potential to provide a substantial increase in wet gas compression control, efficiency -and knowledge. Objects of particular interest is to document the effect of tilting the venturi -and changing the venturies geometry.

Generating larger data sets with more flow regimes, with several volume flows, a number of rotational speeds and different combinations of wet gas flow are needed to create a general digital model for the horizontal venturi.

Bibliography

[1] Collins, A. & Clark, S. 02 2013. Evolution of wet gas venturi metering and wet gas correction algorithms. *Measurement and Control*, 46, 15–20. doi:10.1177/002029401304600102.

[2] ISO/TR 11583:2012 Measurement of wet gas flow by means of pressure differential devices inserted in circular cross-section conduits. URL: https://www.standard.no/en/webshop/search/?search=11583.

[3] Ling, A. L. & Mulyandasari, V. 2011. Compressor selection and sizing (engineering design guideline). *KLM Technology Group*. URL: http://kolmetz.com/pdf/EDG/ENGINEERING%20DESIGN%20GUIDELINES%20-%20Compressors%20REV02.pdf.

[4] Dixon, S. & Hall, C. 2010. *Fluid Mechanics and Thermodynamics of Turbomachinery*. Elsevier Ltd. URL: https://www.sciencedirect.com/book/9781856177931/fluid-mechanics-and-thermodynamics-of-turbomachinery.

[5] Schultz, J. M. 01 1962. The Polytropic Analysis of Centrifugal Compressors. *Journal of Engineering for Power*, 84(1), 69–82. URL: https://doi.org/10.1115/1.3673381.

[6] 2013. Centrifugal compressor map. URL: https://petrowiki.org/File:Vol3_Page_279_Image_0001.png.

[7] King, M. 2016. Compressor control. In *Process Control*, 306–321. John Wiley & Sons, Ltd, Chichester, UK. URL: https://ebookcentral.proquest.com/lib/ntnu/reader.action?docID=4524948.

[8] Andrew, H., Douglas, G., & Richard, S. 2007. A discussion on wet gas flow parameter definitions. In *Proceedings of 25th North Sea Flow Measurement Workshop*. URL: https://nfogm.no/wp-content/uploads/2019/02/2007-08-A-Discussion-on-Wet-Gas-Flow-Parameter-Definitions-Hall-BP.pdf.

[9] ISO 5167:2003 Measurement of fluid flow by means of pressure differential devices inserted in circular cross-section conduits running full. URL: https://www.standard.no/en/webshop/search/?search=5167.

[10] Ian, M, W. & Paul, D. 2003. Penguin wet gas measurement. *North Sea Flow Measurement Workshop 28th – 31st October 2003*. URL: https://nfogm.no/wp-content/uploads/2019/02/2003-05-Penguin-Wet-Gas-Measurement-Wood-Shell.pdf.

[11] Munari, E. & Pinelli, M. 2018. A review of wet gas flow rate measurements by means of singlephase meters. In *Proceedings of the ASME Turbo Expo*, volume 9.

American Society of Mechanical Engineers (ASME). URL: https://doi.org/10.1115/GT2018-76190.

[12] Bjørner, M. G., Fosbol, P. L., Lisberg, M., & Lisberg, H. 2017. Generalized wet gas venturi meter correlations : Assessment and improvement. In *35th North Sea Flow Measurement Workshop*. URL: https://nfogm.no/wp-content/uploads/2019/02/2017-15-Generalized-Wet-Gas-Venturi-Meter-Correlations-Assessment-Bj%C3%B8rner-Emco-Control.pdf.

[13] *Integrated Wet Gas Compressor Test Facility*, volume Volume 9: Oil and Gas Applications; Supercritical CO2 Power Cycles; Wind Energy of *Turbo Expo: Power for Land, Sea, and Air*, 06 2015. V009T24A011. URL: https://doi.org/10.1115/GT2015-43004, arXiv:https://asmedigitalcollection.asme.org/GT/proceedings-pdf/GT2015/56802/V009T24A011/4239187/v009t24a011-gt2015-43004.pdf, doi:10.1115/GT2015-43004.

[14] ASME. 1997. PTC 10: Performance Test Code on Compressors and Exhausters .

[15] *Wet Gas Compressor Operation and Performance*, volume Volume 6A: Energy of *ASME International Mechanical Engineering Congress and Exposition*, 11 2018. V06AT08A056. URL: https://doi.org/10.1115/IMECE2018-86562, arXiv:https://asmedigitalcollection.asme.org/IMECE/proceedings-pdf/IMECE2018/52071/V06AT08A056/2503054/v06at08a056-imece2018-86562.pdf, doi:10.1115/IMECE2018-86562.

[16] *Volute Flow Influence on Wet Gas Compressor Performance*, volume Volume 1: Compressors, Fans and Pumps; Turbines; Heat Transfer; Combustion, Fuels and Emissions of *Gas Turbine India Conference*, 12 2017. V001T01A004. URL: https://doi.org/10.1115/GTINDIA2017-4529, arXiv:https://asmedigitalcollection.asme.org/GTINDIA/proceedings-pdf/GTINDIA2017/58509/V001T01A004/2439507/v001t01a004-gtindia2017-4529.pdf, doi:10.1115/GTINDIA2017-4529.

[17] Mehlum, O. 2019. Experimental analysis of venturi-tube behavior in wet gas conditions. *NTNU Open*. URL: https://ntnuopen.ntnu.no/ntnu-xmlui/handle/11250/2656756.

[18] Bell, I. H., Wronski, J., Quoilin, S., & Lemort, V. 2014. Pure and pseudo-pure fluid thermophysical property evaluation and the open-source thermophysical property library coolprop. *Industrial & Engineering Chemistry Research*, 53(6), 2498–2508. URL: http://pubs.acs.org/doi/abs/10.1021/ie4033999, arXiv:http://pubs.acs.org/doi/pdf/10.1021/ie4033999, doi:10.1021/ie4033999.

[19] Hundseid, O., Bakken, L., Gruner, T., Brenne, L., & Bjorge, T. 01 2008. Wet gas performance of a single stage centrifugal compressor. In *ASME Turbo Expo 2008*, 661–670. doi:10.1115/GT2008-51156.

[20] Fabbrizzi, M., Cerretelli, C., Medico, F., & D'Orazio, M. 01 2009. An experimental

investigation of a single stage wet gas centrifugal compressor. In *ASME Turbo Expo 2009: Power for Land, Sea, and Air, Orlando, Florida, USA, 2009*, volume 5. doi:10.1115/GT2009-59548.

[21] READER-HARRIS, M. J., H. D. G. J. 2006. Venturi-tube performance in wet gas using different test fluids. *North sea flow mesurment workshop*.

[22] Charles Britton, Josh Kinney, R. S. 2008. Liquid property and diameter effect on dp meter wet gas over-readings. *North sea flow mesurment workshop*.

Appendix A Accuracy and operational range of the NTNU compressor laboratory

Instrument section	*Accuracy*	*Unit*
Ambient temperature	± 0.2	°C
Ambient pressure	± 0.15	hPa
Relative humidity	± 1	%
Temperature flow element	± 0.15	°C
Pressure diff. flow element	± 0.04	%
Dynamic pressure diffuser	0.14	mbar
Static pressure diffuser	0.002	bar
Total temperature diffuser	0.009	°C
Three hole probe diffuser	0.11	%
Inlet pressure compressor	± 0.3	%
Inlet temperature compressor	± 0.005	°C
Outlet pressure compressor	± 0.3	%
Outlet temperature compressor	± 0.006	°C
Water flow meter	± 0.5	%
Shaft speed	± 5	%
Shaft torque	± 0.05	%

Figure 36: Accuracy of measurement devices on the NTNU compressor lab [13]

Suction conditions	Atmospheric
Test fluids	Air/water
Air-flow range	0-3 kg/s
Water-flow range	0-5 kg/s
GVF range	99.93 -100%
GMF range	40-100%

Figure 37: Operational range for the NTNU compressor laboratory [13]

Appendix B Test procedure

Appendix B.1 Test procedure for case 1.3

1. If first test of the day perform a still test described in 5.8.
2. Use NTNU/SINTEF start-up procedure for the compressor system.
3. Gradually increase the rotational speed to 9 000 rpm with discharge valve at 100% opening.
4. Adjust discharge valve to desired opening. If multiple discharge valve openings will be tested, start with the highest valve opening.
5. When the modified criteria from PTC-10 is reached, adjust valve opening to next highest opening in the test matrix.
6. Repeat step 4 and 5 until all desired valve openings are tested.
7. Initiate shutdown.

Appendix B.2 Test procedure for case 2

1. If first test of the day perform a still test described in 5.8.
2. Use NTNU/SINTEF start-up procedure for the compressor system.
3. Gradually increase the rotational speed to 9 000 rpm with discharge valve at 100% opening and with no water injection.
4. Adjust discharge valve to desired opening. If multiple discharge valve openings will be tested, start with the highest valve opening.
5. Open and adjust water injection to desired GMF is reached. If multiple GMFs will be tested, start with the highest GMF.
6. After 5 minutes, adjust the water injection to next highest GMF in the test matrix.
7. Repeat step 5 and 6 until all desired GMF are tested for the specific valve opening.
8. Adjust valve opening to next highest opening in the test matrix.
9. Repeat step 5, 6, 7 and 8 until all desired valve openings are tested.
10. Initiate shutdown.

Appendix B.3 Test procedure for case 4

1. If first test of the day perform a still test described in 5.8.
2. Use NTNU/SINTEF start-up procedure for the compressor system.
3. Gradually increase the rotational speed to 9 000 rpm with discharge valve at 100% opening and with no water injection.
4. Adjust discharge valve to 54% opening.
5. Open and adjust water injection to desired GMF is reached. If multiple GMFs will be tested, start with the highest GMF.
6. Wait 15 minutes.
7. Use high speed sampling interval for 2 minutes.
8. Adjust the water injection to next highest GMF in the test matrix.
9. Repeat step 5, 6, 7 and 8 until all desired GMFs are tested.
10. Initiate shutdown.

Appendix B.4 Test procedure for case 6

1. If first test of the day perform a still test described in 5.8.
2. Use NTNU/SINTEF start-up procedure for the compressor system.
3. Gradually increase the rotational speed to 9 000 rpm with discharge valve at 100% opening and with no water injection.
4. Adjust discharge valve to 54% opening.
5. Open and adjust water injection to desired GMF is reached. If multiple GMFs will be tested, start with the highest GMF.
6. Wait 15 minutes.
7. Use high speed sampling interval for 1 minutes.
8. Adjust the water injection to next highest GMF in the test matrix.
9. Repeat step 5, 6, 7 and 8 until all desired GMFs are tested.
10. Initiate shutdown.

Appendix C Data for model validations

Table 6 shows the essential measurement data gathered from case:1.3 described in 5.2.2. The temperature and pressure measurements before and after the compressor are averages of 4 sensors each. The power is calculated from TQ and the rotational speed and Mas flow is calculated P_{o-DP} in accordance with ISO 5167-2.

Table 6: Data for model validation

Data form case:1.3		
P_{o-DP}	40.98	mbar
P_o	992.43	mbar
T_o	25.63	°C
P_1	951.26	mbar
T_1	26.72	°C
P_2	1151.5	mbar
T_2	46.32	°C
RH_{atm}	32.98	%
TQ	30.48	Nm
Power	28.73	KW
Mass flow	1.30	Kg/s

Appendix D Mass flow calculations

```
1 import math
2 import CoolProp.CoolProp as CP
3 import CoolProp.Plots as CPP
4 import CoolProp.HumidAirProp as HCP
5 import matplotlib.pyplot as plt
6 m_ori=1#First gues for iterativ loop
7
8 gas='Air'
9 liq='Water'
10 R=0.484 # humidity
11 T_amb=273.15+25
12 P_amb=99405
13 Tliq=273.15+11.9
14 Tgas=273.15+25.97
15 Pgas_ori=98867
16 dpPgas_ori=37.73
17 Pgas_ven=95124
18 dpPgas_ven=21.46
19 Pliq=101325
20 v_liq=0.343
21
22 m_liq=CP.PropsSI('D','T',Tliq,'P',Pliq,liq)*v_liq/1000
23 beta=160/250
24 d_ori=0.16
25 d_ven=0.15
26 D_ori=0.25
27 D_ven=0.23
28 k_ven=CP.PropsSI('isentropic_expansion_coefficient','T',Tga
   s,'P',Pgas_ven,gas)
29 a=0.909893 #Factor for nitrogen water
30 b=32.680548 #Factor for nitrogen water
31 beta_ven=15/23
32 #GMF=0.90
33 L1=0 #Orifis pressur tapping factor from ISO5167
34 L2=0 #Orifis pressur tapping factor from ISO5167
35 M2=2*L2/(1-beta)#Orifis pressur tapping factor
36 m_humid=HCP.HAPropsSI('W','T',T_amb,'P',P_amb,'R',R)
37 c_ven=0.995
38 t=(Pgas_ven-dpPgas_ven*100)/Pgas_ven
```

```
39 densgas_ori=(1/HCP.HAPropsSI('Vha','T',Tgas,'P',Pgas_ori,'W
   ',m_humid))
40 densgas_ven=(1/HCP.HAPropsSI('Vha','T',Tgas,'P',Pgas_ven,'W
   ',m_humid))
41 dyn_viscos_ori=HCP.HAPropsSI('Visc','T',Tgas,'P',Pgas_ori,'
   W',m_humid) #humid viscosity
42 for i in range(10):
43     ReD_ori=m_ori*4/(math.pi*dyn_viscos_ori*D_ori)
44     c_ori=0.5961+0.0261*beta**2-0.216*beta**8+0.000521*(100
       0000*beta/ReD_ori)48 **0.7+(0.0188+0.0063*(19000*beta/R
       eD_ori)**0.8)*beta**3.5*(1000000/ReD_ori)**0.3+(0.043+0
       .080*math.exp(-10*L1)-0.123*math.exp(-7*L1))*(1-0.11*(1
       9000*beta/ReD_ori)**0.8)*beta**4/(1-beta**4)-0.031*(M2-
       0.8*M2**1.1)*beta**1.3
45     eta_ori=1-(0.351+0.256*beta**4+0.93*beta**8)*(1-((Pgas_
       ori-dpPgas_ori)/Pgas_ori)**(1/1.4))
       # expansibility factor from ISO 5167-2
46     m_ori= densgas_ori*eta_ori*c_ori*(math.pi/4)*d_ori**2*(
       (2*dpPgas_ori*10**2/densgas_ori)/(1-beta**4))**0.5
47     eta_ven=((k_ven*t**(2/k_ven)/(k_ven-1))*((1-beta_ven**4
       )/(1-beta_ven**4*t**(2/k_ven)))*(1-t**((k_ven-1)/k_ven)
       )/(1-t))**0.5 # expansibility factor from ISO 5167-4
48     m_ven= eta_ven*c_ven*(math.pi/4)*d_ven**2*((2*dpPgas_ve
       n*10**2*densgas_ven)/(1-beta_ven**4))**0.5
49 print('m orifice=',m_ori)
50 print('m venturi=',m_ven)
51
52
53 densliq=CP.PropsSI('D','T',Tliq,'P',Pliq,liq)
54 DR=densgas_ven/densliq
55 m_ven_corection=m_ven
56 for i in range(10):
57     X=(m_liq/m_ven_corection)*math.sqrt(densgas_ven/densliq
       )
58     Frgas=(4*m_ven_corection)/(densgas_ven*math.pi*D_ven**2
       *math.sqrt(9.81*D_ven))*math.sqrt(densgas_ven/(densliq-
       densgas_ven))
59     var=math.sqrt(X/0.016)
60     if math.sqrt(X/0.016)>1:
61         var=1
62     C=1-0.0463*math.exp(-0.05*Frgas/(beta**2.5))*var
63     if v_liq==0:
64         C=0.995
65     n=0.583-0.18*beta**2-0.578*math.exp(-0.8*Frgas/1.35)
```

```
66      if n<0.392-0.18*beta**2:
67          n=0.392-0.18*beta**2
68      Cch=(densliq/densgas_ven)**n+(densgas_ven/densliq)**n
69      Overread=math.sqrt(1+Cch*X+X**2)+a*(Cch-2)*X*math.exp(-
        b*X)
70      m_ven_ny=eta_ven*C*(math.pi/4)*d_ven**2*((2*dpPgas_ven*
        10**2*densgas_ven)/(1-beta_ven**4))**0.5
71      m_ven_corection=m_ven_ny/Overread
72      GMF=m_ven_corection/(m_ven_corection+m_liq)
73
74 print('Overreading =',Overread)
75 print('Corected masflow =',m_ven_corection)
76 print('GMF =',GMF)
77
78 Qair=m_ori/HCP.HAPropsSI('Vha','T',273.15+22,'P',94400,'W',
   m_humid)
79 print('Qair=',Qair)
80 print('diferens of m_ven and m_ori =',((m_ori)/m_ven_corect
   ion)**(-1))
```

Appendix E How to play videos in the PDF

If the pdf video won't play, download Foxit reader from https://www.foxitsoftware.com/pdf-reader/. Install the reader and disable safe reading mode under file → Preferences → Trust Manager as depicted in figure 38

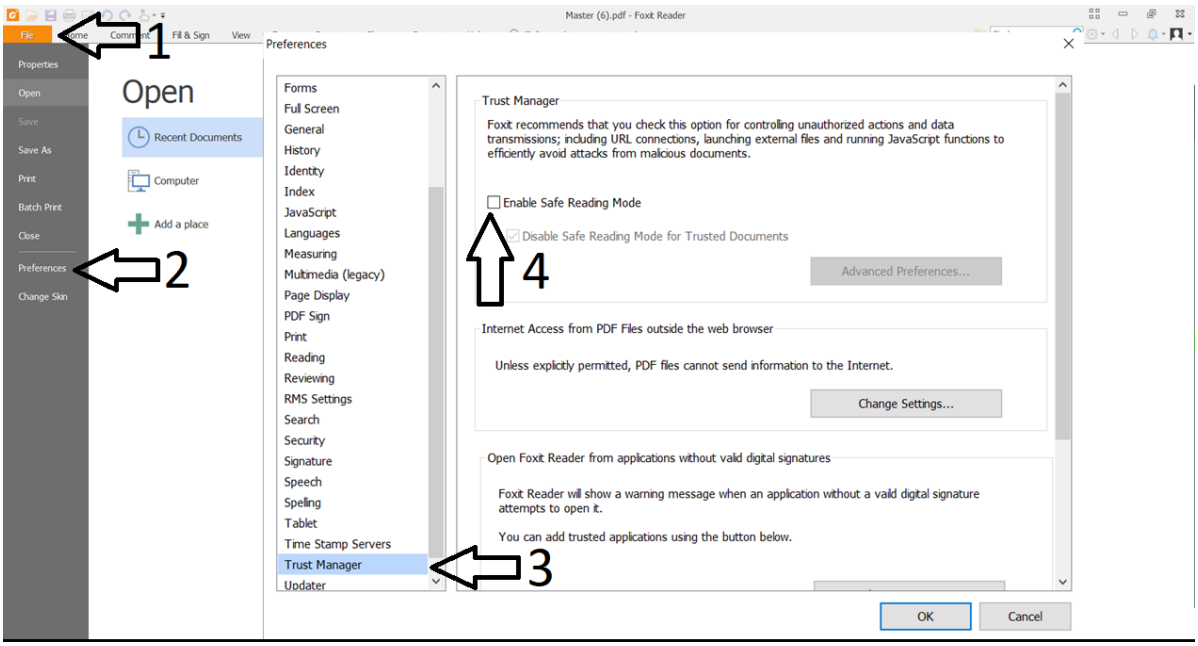

Figure 38: How to allow PDF reader to play videos

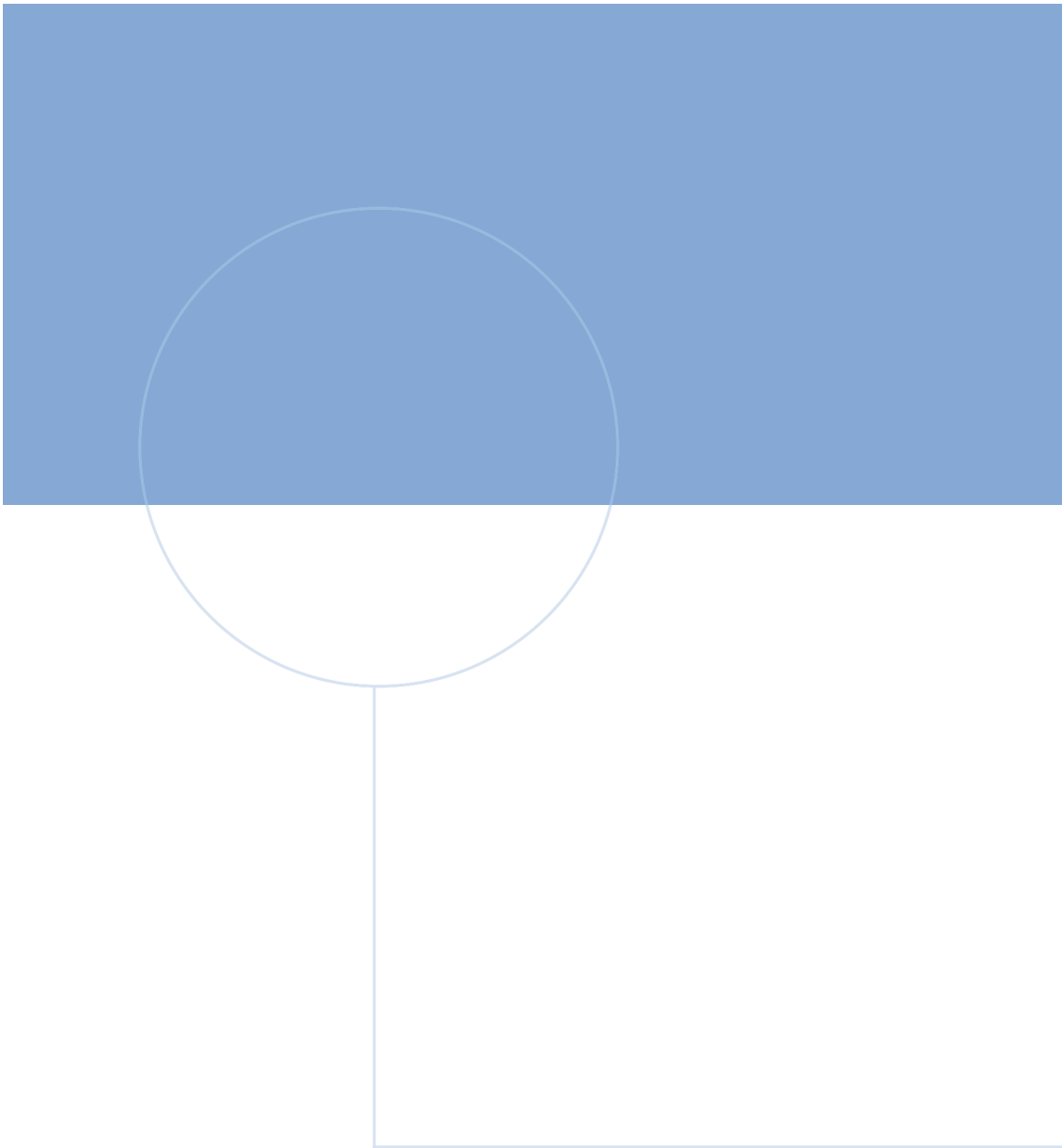

NTNU

Norwegian University of
Science and Technology